

# Methane, carbon dioxide, and nitrous oxide emissions from two clear-water and two turbid-water urban ponds in Brussels (Belgium)

Thomas Bauduin <sup>1,2</sup>, Nathalie Gypens <sup>1</sup>, Alberto V. Borges <sup>2</sup>

<sup>1</sup>Ecology of Aquatic Systems, Université Libre de Bruxelles, Belgium

<sup>2</sup>Chemical Oceanography Unit, University of Liège, Belgium

Correspondence to: Thomas Bauduin ([thomas.bauduin@ulb.be](mailto:thomas.bauduin@ulb.be)) and Alberto V. Borges ([alberto.borges@uliege.be](mailto:alberto.borges@uliege.be))

**Abstract.** Shallow ponds can occur either in a clear-water state dominated by macrophytes or a turbid-water state dominated by phytoplankton, but it is unclear if and how these two alternative states affect the emission of greenhouse gases (GHGs) such as carbon dioxide (CO<sub>2</sub>), methane (CH<sub>4</sub>), and nitrous oxide (N<sub>2</sub>O) to the atmosphere. We measured the dissolved concentration of CO<sub>2</sub>, CH<sub>4</sub>, and N<sub>2</sub>O from which the diffusive air-water fluxes were computed, in four urban ponds in the city of Brussels (Belgium): two clear-water macrophyte-dominated ponds (Silex and Tenreuken), and two turbid-water phytoplankton-dominated ponds (Leybeek and Pêcheries) on 46 occasions over 2.5 years (between June 2021 and December 2023). Ebullitive CH<sub>4</sub> fluxes were measured with bubble traps in the four ponds during deployments in spring, summer, and fall, totalling 48 days of measurements. Measured ancillary variables included water temperature, oxygen saturation level (%O<sub>2</sub>), concentrations of chlorophyll-*a* (Chl-*a*), total suspended matter (TSM), soluble reactive phosphorus (SRP), nitrite (NO<sub>2</sub><sup>-</sup>), nitrate (NO<sub>3</sub><sup>-</sup>), and ammonium (NH<sub>4</sub><sup>+</sup>). The turbid-water and clear-water ponds did not differ significantly in terms of diffusive emissions of CO<sub>2</sub> and N<sub>2</sub>O. Clear-water ponds exhibited higher values of ebullitive CH<sub>4</sub> emissions compared to turbid-water ponds, most probably in relation to the delivery of organic matter from macrophytes to sediments, but the diffusive CH<sub>4</sub> emissions were not significantly different between clear- and turbid-water ponds. Across seasons, CH<sub>4</sub> emissions increased with water temperature in all four ponds, with ebullitive CH<sub>4</sub> fluxes having a stronger dependence on water temperature (Q<sub>10</sub>) than diffusive CH<sub>4</sub> fluxes. The temperature sensitivity of ebullitive CH<sub>4</sub> fluxes decreased with increasing water depth, implying that shallow sediments would respond more strongly to warming (*e.g.* heat waves). Total annual CH<sub>4</sub> emissions (diffusive+ebullitive) in CO<sub>2</sub> equivalents equalled those of CO<sub>2</sub> in turbid-water ponds and exceeded those of CO<sub>2</sub> in clear-water ponds, while N<sub>2</sub>O emissions were negligible compared to the other two GHGs. Total annual GHG emissions in CO<sub>2</sub> equivalents from all four ponds increased from 2022 to 2023 due to higher CO<sub>2</sub> diffusive fluxes, likely driven by higher annual precipitation in 2023 compared to 2022 (leading putatively to higher inputs for organic or inorganic carbon from run-off), possibly in response to the intense El Niño event of 2023. The findings of this work suggest that it might be necessary to account for the presence of submerged macrophytes when extrapolating ebullitive CH<sub>4</sub> fluxes in ponds at larger scale (regional or global) (particularly if Chl-*a* is used as a descriptor), although it might be less critical for the extrapolation of diffusive CH<sub>4</sub>, CO<sub>2</sub>, and N<sub>2</sub>O fluxes.

## 1. Introduction

Greenhouse gas (GHG) emissions from inland water (rivers, lakes, and reservoirs) to the atmosphere such as carbon dioxide (CO<sub>2</sub>), methane (CH<sub>4</sub>), and nitrous oxide (N<sub>2</sub>O) are quantitatively important for global budgets (Lauerwald et al., 2023). Global GHG emissions from lakes are lower than from rivers for CO<sub>2</sub> (Raymond et al., 2013) and for N<sub>2</sub>O (Lauerwald et al., 2019; Maavara et al., 2019). However, reported global emissions of CH<sub>4</sub> from lakes (Rosentreter et al., 2021; Johnson et al., 2022) are equivalent or even higher compared to rivers (Stanley et al., 2016; Rocher-Ros et al., 2023). Global emissions of

CO<sub>2</sub> and CH<sub>4</sub> from lakes to the atmosphere represent 1.25 to 2.30 Pg CO<sub>2</sub> equivalents (CO<sub>2</sub>-eq) annually with a significant proportion from CH<sub>4</sub> emissions, and represent nearly 20% of global CO<sub>2</sub> emissions from fossil fuels (Delsontro et al., 2018). The contribution of CO<sub>2</sub> and CH<sub>4</sub> emissions from small lentic water bodies (small lakes and ponds) can be disproportionately high compared to large systems (Holgerson and Raymond, 2016) as small lakes and ponds are the most abundant of all water body types in number (Verpoorter et al., 2014; Cael et al., 2017), and fluxes per m<sup>2</sup> are usually higher from smaller water bodies. The emissions of GHGs from artificial water bodies such as agricultural reservoirs, urban ponds, and storm-water retention basins could be higher than those from natural systems (Martinez-Cruz et al., 2017; Grinham et al., 2018; Herrero Ortega et al., 2019; Gorsky et al., 2019; Ollivier et al., 2019; Peacock et al., 2019, 2021; Webb et al., 2019; Bauduin et al., 2024). These higher GHG emissions seem to result from higher external inputs of anthropogenic organic carbon and dissolved inorganic nitrogen (DIN) into artificial systems, but might also reflect other differences compared to natural systems such as in hydrology (Clifford and Heffernan, 2018). Among artificial systems, urban ponds are the subject of a growing body of literature on GHG emissions (Singh et al., 2000; Natchimuthu et al., 2014; van Bergen et al., 2019; Audet et al., 2020; Peacock et al., 2021; Goeckner et al., 2022; Ray and Holgerson, 2023; Ray et al. 2023; Bauduin et al., 2024). Urban areas can have numerous small artificial water bodies mostly associated to green spaces such as public parks, and their number is increasing due to rapid urbanisation worldwide (Brans et al., 2018; Audet et al., 2020; Gorsky et al., 2024; Rabaey et al., 2024). Urban ponds are generally small, shallow, and usually their catchment consists in majority of impervious surfaces with a smaller contribution from soils (Davidson et al., 2015; Peacock et al., 2021). In general, the main function of urban ponds is for storm-water management but they provide additional benefits including aesthetic/recreational amenities and habitats for wildlife (e.g. Tixier et al., 2011; Hassall, 2014).

Shallow ponds and lakes occur in two alternative states corresponding to systems with either clear waters (macrophyte-dominated) or turbid waters (phytoplankton-dominated), during the productive period of the year (spring and summer in mid-latitudes) (Scheffer et al., 1993). Submerged macrophytes and phytoplankton regulate CO<sub>2</sub> dynamics directly through photosynthesis that can be more or less balanced by community respiration in the water column (*e.g.*, Sand-Jensen and Staehr, 2007). However, it is not clear whether the presence of macrophytes increases or decreases the net CO<sub>2</sub> emissions from ponds and lakes. Some studies have shown a decrease of CO<sub>2</sub> emissions with increasing macrophyte density (Kosten et al., 2010; Ojala et al., 2011; Davidson et al., 2015), but other studies showed the opposite pattern (Theus et al., 2023). In phytoplankton-dominated lakes, CO<sub>2</sub> concentrations depend in part on the developmental stage of phytoplankton, with the growth and peak phases generally coinciding with lower CO<sub>2</sub> concentrations due to photosynthesis (Grasset et al., 2020; Vachon et al., 2020).

CH<sub>4</sub> emissions have been reported to increase with the concentration of chlorophyll-*a* (Chl-*a*) in phytoplankton-dominated lakes (DelSontro et al., 2018; Borges et al., 2022). The presence of macrophytes strongly affects the production of CH<sub>4</sub> in freshwaters (Bastviken et al., 2023) and vegetated littoral zones of lakes exhibit higher CH<sub>4</sub> emissions than non-vegetated zones (Hyvönen et al., 1998; Huttunen et al., 2003; Juutinen et al., 2003; Desrosiers et al., 2022; Theus et al., 2023). Macrophytes influence organic matter decomposition processes in sediments depending on the quality and quantity of plant matter they release into their environment (Reitsema et al., 2018; Grasset et al., 2019; Harpenslager et al., 2022; Theus et al., 2023). Yet, few studies have consistently compared CH<sub>4</sub> emissions in clear-water and turbid-water ponds (Hilt et al., 2017). A study in Argentina reported higher dissolved CH<sub>4</sub> concentrations in clear-water ponds with submerged macrophytes compared to turbid-water phytoplankton-dominated ponds, but no differences in measured CH<sub>4</sub> emissions (Baliña et al., 2023).

76 The production of N<sub>2</sub>O predominantly occurs through microbial nitrification and denitrification that depend on DIN, O<sub>2</sub>  
77 levels, and temperature (Codispoti and Christensen, 1985; Mengis et al., 1997; Velthuis and Veraart, 2022). Competition for  
78 DIN between primary producers and N<sub>2</sub>O-producing microorganisms can impact N<sub>2</sub>O production. Additionally, the transfer  
79 of labile phytoplankton organic matter to sediments fuels benthic denitrification and impacts N<sub>2</sub>O fluxes. Eutrophication is  
80 assumed to drive high N<sub>2</sub>O emissions from lakes and ponds (Audet et al., 2020; Webb et al., 2021; Wang et al., 2021; Xie et  
81 al., 2024) but some lakes with elevated Chl-*a* concentrations can act as sinks of N<sub>2</sub>O due to removal of N<sub>2</sub>O by  
82 denitrification (Webb et al., 2019; Borges et al., 2022; 2023). The presence of macrophytes also strongly influences nitrogen  
83 cycling in sediments of lakes and ponds (Barko et al., 1991; Choudhury et al., 2018; Deng et al., 2020; Dan et al., 2021) and  
84 should in theory also affect N<sub>2</sub>O emissions, although seldom investigated, and available studies provide contradictory  
85 conclusions. N<sub>2</sub>O emissions have been shown to follow diurnal cycles of O<sub>2</sub> concentrations in areas dominated by  
86 submerged macrophytes in Lake Wuliangsuhai (China) (Ni et al., 2022) and the seasonal cycle of aboveground biomass of  
87 emerged macrophytes (*Phragmites*) in Baiyangdian Lake (China) (Yang et al., 2012). On the contrary, a study showed there  
88 was no significant difference of N<sub>2</sub>O production in sediments of macrophyte-rich (n=10) and macrophyte-free (n=12) lakes  
89 in subtropical China (Liu et al., 2018). There has been a very limited number of studies systematically investigating how  
90 emissions differ between ponds dominated by phytoplankton and those dominated by macrophytes (Baliña et al., 2023), and  
91 none investigating simultaneously CO<sub>2</sub>, CH<sub>4</sub>, and N<sub>2</sub>O emissions including both diffusive and ebullitive components.

92 The emissions of CO<sub>2</sub> and N<sub>2</sub>O from aquatic systems are exclusively through diffusion across the air-water interface  
93 (diffusive flux), while CH<sub>4</sub> can be additionally emitted as bubbles released from sediments to the atmosphere (ebullitive  
94 flux). At annual scale, ebullitive CH<sub>4</sub> flux usually represents more than half of total (diffusive+ebullitive) CH<sub>4</sub> emissions  
95 from shallow lakes (Wik et al., 2013; Deemer and Holgerson, 2021), although the relative contribution of ebullitive and  
96 diffusive CH<sub>4</sub> emissions is highly variable seasonally (*e.g.* Wik et al., 2013; Ray and Holgerson, 2023; Rabaey and Cotner  
97 2024). Ebullitive CH<sub>4</sub> fluxes are particularly high in the littoral zone of lakes at depths <5 m (Wik et al., 2013; DelSontro et  
98 al., 2016; Borges et al., 2022) and strongly increase in response to temperature (DelSontro et al., 2016; Aben et al., 2017;  
99 Rabaey and Cotner 2024), as well as organic matter availability (DelSontro et al., 2016; 2018). Ebullitive CH<sub>4</sub> fluxes tend to  
100 be higher in small and shallow water bodies (Deemer and Holgerson, 2021) but are notoriously variable in time and space,  
101 and are difficult to estimate reliably (DelSontro et al., 2011).

102 Here, we report a dataset of CO<sub>2</sub>, CH<sub>4</sub>, and N<sub>2</sub>O dissolved concentrations in four shallow and small urban ponds (Leybeek,  
103 Pêcherries, Silex, and Tenreuken) in the city of Brussels (Belgium) (Fig. 1), with data collected 46 times at regular intervals  
104 (between June 2021 and December 2023) on each pond. The air-water diffusive fluxes of CO<sub>2</sub>, CH<sub>4</sub>, and N<sub>2</sub>O were  
105 calculated from dissolved concentrations and the gas transfer velocity, while the ebullitive CH<sub>4</sub> fluxes were measured with  
106 inverted funnels during 8 deployments (totalling 48 days) in the four ponds. The four ponds have similar depth, surface area,  
107 and catchment urban coverage, and mainly differ by the phytoplankton-macrophyte dominance, a clear-water state  
108 dominated by macrophytes and a turbid-water state dominated by phytoplankton (alternative states) (Fig. 1). We assess  
109 whether the differences in terms of (i) CO<sub>2</sub>, CH<sub>4</sub>, and N<sub>2</sub>O dissolved concentration and diffusive emissions; (ii) ebullitive  
110 CH<sub>4</sub> emissions; (iii) relative contribution of CO<sub>2</sub>, CH<sub>4</sub>, and N<sub>2</sub>O to the total GHG emissions in CO<sub>2</sub>-eq between the four  
111 ponds are explained by the two alternative states.

## 112 2. Material and Methods

### 113 2.1. Field sampling and meteorological data

114 Sampling was carried out at a single fixed station (pontoon) in each of the four ponds, on the same day between 9am and  
115 11am, 46 times on each pond between June 2021 and December 2023 at a frequency ranging from one (winter) to three  
116 (summer) times per month. Water was sampled 5 cm below the surface with 60 ml polypropylene syringes for analysis of  
117 dissolved concentrations of CO<sub>2</sub>, CH<sub>4</sub>, and N<sub>2</sub>O. Samples for CH<sub>4</sub> and N<sub>2</sub>O were transferred from the syringes with a silicone  
118 tube into 60 ml borosilicate serum bottles (Wheaton), preserved with 200 µl of a saturated solution of HgCl<sub>2</sub>, sealed with a  
119 butyl stopper and crimped with aluminium cap, without a headspace, and stored at ambient temperature in the dark prior to  
120 analysis in the laboratory. The partial pressure of CO<sub>2</sub> (pCO<sub>2</sub>) was measured directly in the field, within 5 minutes of sample  
121 collection, with a Li-Cor Li-840 infrared gas analyser (IRGA) based on the headspace technique with 4 polypropylene  
122 syringes (Borges et al., 2019). A volume of 30 ml of sample water was equilibrated with 30 ml of atmospheric air within the  
123 syringe by shaking vigorously for 5 minutes. The headspace of each syringe was then sequentially injected into the IRGA  
124 and a fifth syringe was used to measure atmospheric CO<sub>2</sub>. The final pCO<sub>2</sub> value was computed taking into account the  
125 partitioning of CO<sub>2</sub> between water and the headspace, as well as equilibrium with HCO<sub>3</sub><sup>-</sup> (Dickson et al., 2007) using water  
126 temperature measured in-situ and after equilibration, and total alkalinity (data not shown). Samples for total alkalinity were  
127 conditioned, stored, and analysed as described by Borges et al. (2019). The IRGA was calibrated in the laboratory with  
128 ultrapure N<sub>2</sub> and a suite of gas standards (Air Liquide Belgium) with CO<sub>2</sub> mixing ratios of 388, 813, 3788 and 8300 ppm.  
129 The precision of pCO<sub>2</sub> measurements was ±2.0%. Water temperature, specific conductivity, and oxygen saturation level  
130 (%O<sub>2</sub>) were measured in-situ with VWR MU 6100H probe 5 cm below the surface. A 2 liter polyethylene water container  
131 was filled with surface water for conditioning the samples for other variables at the laboratory in Université Libre de  
132 Bruxelles.

133 Three bubble traps were deployed 50 cm apart for measuring ebullitive CH<sub>4</sub> flux. The bubble traps consisted of inverted  
134 polypropylene funnels (diameter 23.5 cm) mounted with 60 ml polypropylene syringes, with three way stop valves allowing  
135 to collect the gas without contamination from ambient air. The polypropylene funnel was attached with steel rods to a  
136 polystyrene float. The volume of gas collected in the funnels was sampled with graduated polypropylene 60 ml syringes  
137 every 24 hours. The value of the collected volume of gas was logged, and the gas was transferred immediately after  
138 collection to pre-evacuated 12 ml vials (Exetainers, Labco, UK) that were stored at ambient temperature in the dark prior to  
139 the analysis of CH<sub>4</sub> concentration in the laboratory. The time-series of measurements was longer at the Silex pond than the  
140 other three ponds.

141 Surveys to identify and quantify visually the relative coverage of emerged and submerged macrophytes were conducted in  
142 summer 2023 (Table S1). The resulting list of macrophyte species agreed with past studies in Brussels' ponds (Peretyatko et  
143 al., 2007). Air temperature, precipitation, wind speed, and atmospheric pressure, were retrieved from  
144 <https://wow.meteo.be/en> for the meteorological station of the Royal Meteorological Institute of St-Lambert (50.8408°N,  
145 4.4234°E) in Brussels, located between 2.5 and 5.0 km from the surveyed ponds. Air temperature, wind speed and  
146 atmospheric pressure were averaged over 24 h to obtain a daily mean value. Precipitation was integrated each day to obtain  
147 cumulated daily value.

## 148 2.2. Laboratory analysis

### 149 2.2.1. Chlorophyll-*a*, total suspended matter, and dissolved inorganic nutrients

150 Water was filtered through Whatman GF/F glass microfiber filters (porosity 0.7 µm) with a diameter of 47 mm for total  
151 suspended matter (TSM) and Chl-*a*. Filters for TSM were dried in an oven at 50 °C and filters for Chl-*a* were kept frozen (-  
152 20 °C). The weight of each filter was determined before and after filtration of a known volume of water using an Explorer™  
153 Pro EP214C analytical microbalance (accuracy ±0.1 mg) for determination of TSM concentration. Chl-*a* concentration was  
154 measured on extracts with 90% acetone by fluorimetry (Kontron model SFM 25) (Yentsch and Menzel, 1963) with a limit of  
155 detection of 0.01 µg L<sup>-1</sup>. Filtered water was stored frozen (-20 °C) in 50 ml polypropylene bottles for analysis of dissolved  
156 nutrients. Soluble reactive phosphorus (SRP) was determined by the ammonium molybdate, ascorbic acid and potassium  
157 antimony tartrate staining method (Koroleff, 1983), with a limit of detection of 0.1 µmol L<sup>-1</sup>. Ammonium (NH<sub>4</sub><sup>+</sup>) was  
158 determined by the nitroprusside-hypochlorite-phenol staining method (Grasshoff and Johannsen, 1972), with a limit of  
159 detection of 0.05 µmol L<sup>-1</sup>. Nitrite (NO<sub>2</sub><sup>-</sup>) and nitrate (NO<sub>3</sub><sup>-</sup>) were determined before and after reduction of NO<sub>3</sub><sup>-</sup> to NO<sub>2</sub><sup>-</sup> by a  
160 cadmium-copper column, using the Griess acid reagent staining method (Grasshoff et al., 2009), with a detection limit of  
161 0.01 and 0.1 µmol L<sup>-1</sup>, respectively. Concentration of dissolved inorganic nitrogen (DIN) was calculated as the sum of NH<sub>4</sub><sup>+</sup>,  
162 NO<sub>2</sub><sup>-</sup> and NO<sub>3</sub><sup>-</sup> concentrations in µmol L<sup>-1</sup>.

### 163 2.2.2. CH<sub>4</sub> and N<sub>2</sub>O measurements by gas chromatography

164 Measurements of N<sub>2</sub>O and CH<sub>4</sub> concentrations dissolved in water were made with the headspace technique (Weiss, 1981)  
165 with an headspace volume of 20 ml of ultra-pure N<sub>2</sub> (Air Liquid Belgium) and a gas chromatograph (GC) (SRI 8610C) with  
166 a flame ionisation detector for CH<sub>4</sub> and an electron capture detector for N<sub>2</sub>O calibrated with CH<sub>4</sub>:N<sub>2</sub>O:N<sub>2</sub> gas mixtures (Air  
167 Liquide Belgium) with mixing ratios of 1, 10 and 30 ppm for CH<sub>4</sub>, and 0.2, 2.0 and 6.0 ppm for N<sub>2</sub>O. The precision of  
168 measurement based on duplicate samples was ±3.9% for CH<sub>4</sub> and ±3.2% for N<sub>2</sub>O. Measurements of CH<sub>4</sub> concentration in the  
169 gas samples from bubble traps were also made by GC with the same set-up and calibration as for the determination of the  
170 dissolved concentrations in water samples.

171 The CO<sub>2</sub> concentration is expressed as partial pressure (pCO<sub>2</sub>) in parts per million (ppm) and CH<sub>4</sub> as dissolved concentration  
172 (nmol L<sup>-1</sup>), as frequently used in topical literature. CH<sub>4</sub> concentration were systematically and distinctly above saturation  
173 level (2-3 nmol L<sup>-1</sup>) and pCO<sub>2</sub> values were below saturation only five times out of the 187 measurements. The N<sub>2</sub>O  
174 concentrations fluctuated around atmospheric equilibrium, so data are presented as percent of saturation level (%N<sub>2</sub>O, where  
175 atmospheric equilibrium corresponds to 100%). The equilibrium with atmosphere for N<sub>2</sub>O was calculated from the average  
176 air mixing ratios of N<sub>2</sub>O provided by the Global Monitoring Division (GMD) of the National Oceanic and Atmospheric  
177 Administration (NOAA) Earth System Research Laboratory (ESRL) (Dutton and Hall, 2023), and using the Henry's  
178 constant given by Weiss and Price (1980).

## 179 2.3. Calculations

### 180 2.3.1. Diffusive GHG emissions

181 The diffusive air-water CO<sub>2</sub>, CH<sub>4</sub>, or N<sub>2</sub>O fluxes ( $F_G$ ) were computed according to:

$$182 \quad F_G = k \times \Delta[G], \quad (1)$$

183 where  $k$  is the gas transfer velocity and  $\Delta[G]$  is the air-water gas concentration gradient.

184 The atmospheric pCO<sub>2</sub> was measured in the field with the Li-Cor Li-840. For CH<sub>4</sub>, the global average present day  
 185 atmospheric mixing ratio of 1.9 ppm was used (Lan et al., 2024).  $k$  was computed from a value normalized to a Schmidt  
 186 number of 600 ( $k_{600}$ ) and from the Schmidt number of CO<sub>2</sub>, CH<sub>4</sub> and N<sub>2</sub>O in freshwater according to the algorithms as  
 187 function of water temperature given by Wanninkhof (1992).  $k_{600}$  was calculated from the parameterization as a function of  
 188 wind speed of Cole and Caraco (1998). CH<sub>4</sub> and N<sub>2</sub>O emissions were converted into CO<sub>2</sub> equivalents (CO<sub>2</sub>-eq) considering a  
 189 100-year timeframe, using global warming potentials of 32 and 298 for CH<sub>4</sub> and N<sub>2</sub>O, respectively (Myrhe et al., 2013).

### 190 2.3.2. Ebullitive flux

191 Bubble flux (ml m<sup>-2</sup> d<sup>-1</sup>) measured with the inverted funnels was calculated according to:

$$192 \quad F_{bubble} = \frac{V_g}{A \times \Delta t}, \quad (2)$$

193 where  $V_g$  is the volume of gas collected in the funnels (ml),  $A$  is the cross-sectional area of the funnel (m<sup>2</sup>),  $\Delta t$  is the  
 194 collection time (d).

195 A multiple linear regression model of  $F_{bubble}$  dependent on water temperature ( $T_w$  in °C) and drops of atmospheric pressure  
 196 ( $\Delta p$  in atm) was fitted to the data according to:

$$197 \quad \log_{10}(F_{bubble}) = \alpha \times T_w + \beta \times \Delta p + \gamma, \quad (3)$$

198 where  $\alpha$  and  $\beta$  are the slope coefficients of the multiple linear regression model,  $\gamma$  is the y-intercept.

199  $\Delta p$  was calculated according to Zhao et al. (2017):

$$200 \quad \Delta p = -\frac{1}{\Delta t} \int_0^t p - p_0; \quad \forall p < p_0, \quad (4)$$

201 where  $p$  is the atmospheric pressure (atm),  $p_0$  a threshold pressure fixed at 1 atm and  $\Delta t$  the time interval between two  
 202 measurements (d) (Fig. S1).

203 A linear regression model of  $F_{bubble}$  dependent on  $T_w$  alone was fitted to the data according to:

$$204 \quad \log_{10}(F_{bubble}) = \alpha' \times T_w + \gamma', \quad (5)$$

205 where  $\alpha'$  is the slope coefficient and  $\gamma'$  is the y-intercept.

206 To evaluate the relative importance of  $T_w$  and  $\Delta p$  in driving  $F_{bubble}$  the modelled based on (3) and on (5) were compared to  
 207 the observations in all four ponds, for three  $T_w$  ranges ( $T_w < 15^\circ\text{C}$ ,  $T_w > 15^\circ\text{C}$ , and the full  $T_w$  range). The  $F_{bubble}$  observations  
 208 clustered for  $T_w <$  and  $> 15^\circ\text{C}$  (see hereafter).

209 Ebullitive CH<sub>4</sub> fluxes (mmol m<sup>-2</sup> d<sup>-1</sup>) were calculated according to:

$$210 \quad E_{CH_4} = [CH_4] \times F_{bubble}, \quad (6)$$

211 where  $[CH_4]$  is the CH<sub>4</sub> concentration in bubbles (mmol ml<sup>-1</sup>).

212 The methane ebullition  $Q_{10}$  represents the proportional change in the ebullitive  $CH_4$  flux per  $10^\circ C$  change in water  
 213 temperature (DelSontro et al., 2016) and was computed according to:

$$214 \quad Q_{10} = 10^{10b}, \quad (7)$$

215 where  $b$  is the slope of the linear regression between the logarithm of the ebullitive  $CH_4$  flux ( $E_{CH_4}$ ) and  $T_w$ , and  $c$  is the y-  
 216 intercept, according to:

$$217 \quad \log_{10}(E_{CH_4}) = b \times T_w + c, \quad (8)$$

218 Equation (8) is used to predict  $E_{CH_4}$  in each pond from measured time-series of  $T_w$  allowing matching to each diffusive  $CH_4$   
 219 estimate derived from Equation (1).

220 The  $Q_{10}$  of diffusive  $CH_4$  fluxes was also computed from equation (7) but replacing  $E_{CH_4}$  by the diffusive  $CH_4$  flux in  
 221 equation (8).

222 The ratio of ebullitive  $CH_4$  flux to total (diffusive + ebullitive)  $CH_4$  flux ( $\frac{E_{bul}}{Tot}$ ) was fitted as a function of  $T_w$  according to  
 223 DelSontro et al. (2016):

$$224 \quad \frac{E_{bul}}{Tot} = \frac{1}{1 + f \times e^{g \cdot T_w}} \quad (9)$$

## 225 **2.4. Statistical analysis**

226 Generalized linear mixed models (GLMMs) were used (1) to relate GHG variables to their putative controls across all ponds  
 227 and (2) to find differences in variables among ponds. For the data-sets covering the whole sampling period (four seasons  
 228 merged), GLMMs were constructed for  $pCO_2$ , dissolved  $CH_4$  concentration,  $\%N_2O$ , bubble flux,  $\%CH_4$  in bubbles, ebullitive  
 229  $CH_4$  fluxes, and diffusive  $CH_4$  fluxes that included  $T_w$ , precipitation,  $\%O_2$ , Chl-*a*, TSM, DIN, SRP as fixed effects, and  
 230 “pond” and “sampling date” as a random effect to account for repeated measurements via the *lme4* package (Bates et al.,  
 231 2015) in R version 4.4.1 (R Core Team, 2021). When comparing data among the four ponds, “sampling date” was used as a  
 232 random effect and post-hoc tests were performed using estimated marginal means (*emmeans* package) to assess pairwise  
 233 differences between ponds. This analysis aimed at investigating the impact on  $CO_2$  concentrations and emissions of  
 234 photosynthesis-respiration from the relationships with Chl-*a*, DIN, SRP, the impact on  $CH_4$  concentrations and diffusive and  
 235 ebullitive emissions of the response of methanogenesis to temperature from the relationship to  $T_w$ , the impact on  $N_2O$   
 236 concentrations and diffusive emissions on DIN availability and  $T_w$ . Data were also compared among ponds separated by  
 237 seasons, but GLMMs did not converge due to insufficient number of data points. Comparisons on  $\log_{10}$ -transformed data  
 238 were then made using repeated measures analysis of variance (ANOVA) with Tukey’s honestly significant difference (HSD)  
 239 post-hoc tests. This analysis aimed at investigating if patterns in data shown by the data analysis with the full data-set (four  
 240 seasons merged) were also observed when analyzing the data separated by seasons.

241 A linear regression model was used to assess the relationship between Chl-*a*, TSM,  $\%O_2$ , SRP, and DIN versus  $T_w$ . This  
 242 analysis aimed at investigating if some of the patterns between GHG variables versus Chl-*a*, TSM,  $\%O_2$ , SRP, and DIN  
 243 might in fact have reflected indirectly a relation between these variables and  $T_w$ . The relationships between the annual  
 244 means of  $CH_4$ ,  $CO_2$  and  $N_2O$  fluxes and the annual means of a subset of variables (Chl-*a*, macrophyte cover, surface area,  
 245 depth) were assessed with linear or quadratic regressions. The modelled bubble fluxes in the Silex pond and in the four

ponds were compared to measured values with a linear regression in order to evaluate the model performance. A linear regression model was used to assess the relationship between anomalies in annual air temperature and annual precipitation, as well as between CH<sub>4</sub> bubble content and bubble flux. The linear regression model and the Pearson correlation coefficient (r) were computed in R version 4.4.1 using the functions *lm* and *cor(method = "pearson")*, respectively. Statistical significance was set at  $p < 0.05$  for all analyses. For comparisons presented on boxplots, significant differences between groups are indicated by lower-case letters.

### 3. Results

#### 3.1. Seasonal variations of meteorological conditions and GHG concentrations

The city of Brussels experiences a temperate climate with mild weather year-round, and evenly distributed abundant precipitation totalling on average 837 mm annually for the reference period 1991-2020. The average annual air temperature was 11 °C, with summer average of 17.9 °C and winter average of 4.1 °C for the reference period 1991-2020. During the sampling period, from June 2021 to December 2023,  $T_w$  in the surface of the four sampled ponds (Leybeek, Pêcheres, Silex, and Tenreuken; Fig. 1) tracked closely the air temperature that ranged between -1.5 and 30.0°C following the typical seasonal cycle at mid-latitudes in the Northern Hemisphere (Fig. S2). Years 2022 and 2023 were about 1 °C warmer than the average for the period 1991-2020 (11 °C), while year 2021 was closer to the long-term average (Fig. 2). Year 2022 was warmer and drier than 2021 and 2023 (Fig. 2), with positive air temperature anomalies observed evenly throughout the year (9 months out of 12) and negative precipitation anomalies in summer, fall, and early winter (Fig. S2). Year 2021 had warmer and drier months in June and September, colder and wetter months in July and August, and was overall wetter and colder than 2022 (Fig. 2). Year 2023 was marked by both positive air temperature and precipitation anomalies (Fig. S2), resulting in a wetter and warmer year than normal and compared to 2021 and 2022 (Fig. 2). Daily wind speed was generally low ( $<1 \text{ m s}^{-1}$ ) except for a windier period in spring 2022 (up to  $5.8 \text{ m s}^{-1}$ , corresponding to the Eunice storm) and in fall 2023 (up to  $9.7 \text{ m s}^{-1}$ , corresponding to the Ciarán storm) (Fig. S2).

The four sampled ponds are situated in the periphery of the city of Brussels, with the Silex pond being bordered by the Sonian Forest (Fig. 1). The four ponds are relatively small (0.7-3.2 ha) and shallow (0.6-1.4 m) and have not been drained or dredged since at least 2018 (Table S2). The four studied ponds had significantly different Chl-*a* concentration values during summer, with the Leybeek pond having higher Chl-*a* ( $78.8 \pm 49.5 \mu\text{g L}^{-1}$ ), followed by the Pêcheres pond ( $19.1 \pm 13.7 \mu\text{g L}^{-1}$ ), the Tenreuken pond ( $3.3 \pm 2.4 \mu\text{g L}^{-1}$ ), and the Silex pond ( $1.0 \pm 1.2 \mu\text{g L}^{-1}$ ) (Figs. 1, 3, Table S3). The Leybeek and Pêcheres ponds with higher summer Chl-*a* concentration had turbid-water (summer TSM =  $48.7 \pm 36.2$  and  $13.7 \pm 10.7 \text{ mg L}^{-1}$ , respectively), and undetectable submerged macrophyte cover in summer (Fig. 1, Table S1). The Tenreuken and Silex ponds with lower summer Chl-*a* concentrations had clear-water (summer TSM =  $4.9 \pm 3.2$  and  $4.0 \pm 3.2 \text{ mg L}^{-1}$ , respectively), and a high total macrophyte cover during summer (68 and 100%, respectively, Fig. 1, Table S1). Seasonally, the highest values of Chl-*a* were observed in summer in the turbid-water Leybeek and Pêcheres ponds, related to algal blooms. Conversely, lowest values of Chl-*a* were observed in summer in the clear-water Tenreuken and Silex ponds (Figs. 1, 3), probably related to competition for dissolved inorganic nutrients with macrophytes.

The %O<sub>2</sub> values ranged from 11 to 191% (Fig. 3). The highest %O<sub>2</sub> values in the four ponds were observed in spring and summer compared to fall and winter owing to aquatic primary production. In summer, %O<sub>2</sub> was significantly higher in the Leybeek pond ( $109 \pm 46\%$ ) characterized by higher Chl-*a* concentration compared to the Pêcheres pond ( $75 \pm 23\%$ ,  $p=0.0212$ ,

Table S3). The lowest average %O<sub>2</sub> was observed in fall in the Pêcherie pond (46±22%) and was significantly lower than in the Leybeek (85±34%, p=0.0146, Table S3) and Silex ponds (81±19%, p=0.0130, Table S3).

The pCO<sub>2</sub> values ranged from 40 to 13,804 ppm (Fig. 3). Undersaturation of CO<sub>2</sub> with respect to atmospheric equilibrium (~410 ppm) was only observed on five occasions out of the 187 measurements, three times in the turbid-water Leybeek pond in summer (40 ppm on 13 August 2021, 220 ppm on 27 June 2022 and 149 ppm on 13 June 2023), and twice in the clear-water Tenreuken pond in spring and summer (383 ppm on 13 August 2021 and 55 ppm on 2 May 2022). Low values of pCO<sub>2</sub> were generally observed in spring and summer and high values of pCO<sub>2</sub> were observed in fall in the four ponds (Fig. 3). In summer, pCO<sub>2</sub> was lower in the Leybeek pond (2187±2012 ppm) than in the Pêcherie (3427±1672 ppm, p=0.0015, Table S3), and the Silex (3222±1175 ppm, p=0.0002, Table S3) ponds. When data were pooled, pCO<sub>2</sub> was negatively influenced by %O<sub>2</sub>, and positively by DIN, SRP, and precipitation (Table S4). In individual ponds, pCO<sub>2</sub> was negatively influenced by %O<sub>2</sub> and positively by precipitation in the four ponds, positively by DIN in the Leybeek pond, by DIN and SRP in the Tenreuken pond, and negatively by Chl-*a* in the Silex pond (Table S5).

The CH<sub>4</sub> dissolved concentrations ranged from 194 to 48,380 nmol L<sup>-1</sup> (Fig. 3) and was always above saturation (~2 nmol L<sup>-1</sup>). High values of CH<sub>4</sub> dissolved concentrations were generally observed in spring and summer and low values of CH<sub>4</sub> dissolved concentrations were generally observed in winter in the four ponds (Fig. 3). In summer, CH<sub>4</sub> dissolved concentration was higher in the Silex pond (4,898±3,384 nmol L<sup>-1</sup>) than in the Pêcherie (2,518±2,105 nmol L<sup>-1</sup>, p=0.0385, Table S3) and the Tenreuken (2,189±1,365 nmol L<sup>-1</sup>, p=0.0055, Table S3) ponds. When data were pooled, dissolved CH<sub>4</sub> concentration was influenced positively by T<sub>w</sub> (Table S4). In individual ponds, CH<sub>4</sub> dissolved concentration was also influenced positively by T<sub>w</sub> in each of the four ponds (Table S5). Additionally, CH<sub>4</sub> dissolved concentration was positively influenced by precipitation in the Leybeek pond and by SRP in the Silex pond, and negatively by DIN in the Pêcherie pond and by Chl-*a* in the Tenreuken and the Silex ponds. (Table S5). These relationships between CH<sub>4</sub> and other variables (SRP, DIN, Chl-*a*) probably indirectly reflected the seasonal variations of these other variables that were also influenced by T<sub>w</sub>. Indeed, DIN was negatively influenced T<sub>w</sub> in the Pêcherie pond; Chl-*a* was negatively influenced by T<sub>w</sub> in the Tenreuken and the Silex ponds; SRP was positively influenced by T<sub>w</sub> in the Silex pond (Table S6).

The %N<sub>2</sub>O values ranged from 32 to 826% (Fig. 3). Undersaturation of N<sub>2</sub>O with respect to atmospheric equilibrium was observed 66 times out of the 187 measurements. Low values of %N<sub>2</sub>O were generally observed in spring and summer and high values of %N<sub>2</sub>O were generally observed in fall and winter in the four ponds (Fig. 3). During spring, %N<sub>2</sub>O was lower in the Pêcherie pond (90±11%) than the Leybeek (138±30%, p=0.0043, Table S3) and the Tenreuken (138±41, p=0.0057, Table S3) ponds. During summer, %N<sub>2</sub>O was lower in the Pêcherie pond (78±17%) than the Leybeek (191±104%, p<0.0001, Table S3) and the Silex (126±49%, p=0.001, Table S3) pond, and lower in the Tenreuken pond (133±106%) than the Leybeek pond (p=0.0219, Table S3). During fall, %N<sub>2</sub>O was lower in the Pêcherie pond (103±33%) than the Leybeek pond (190±70%, p=0.0174, Table S3). For the all sampling period, %N<sub>2</sub>O was lower in the Pêcherie pond (94±28%) than the Leybeek (178±82 %, p<0.0001, Table S7), the Tenreuken (140±77%, p<0.0001, Table S7), and the Silex (144±113%, p<0.0001, Table S7) ponds, and was lower in the Tenreuken pond than the Leybeek pond (p=0.0038, Table S7). When data were pooled, %N<sub>2</sub>O was influenced negatively by T<sub>w</sub> and positively by DIN and NH<sub>4</sub><sup>+</sup> (Table S4). In individual ponds, %N<sub>2</sub>O was influenced negatively by T<sub>w</sub> in the Leybeek, the Pêcherie, and the Tenreuken ponds (Table S5). %N<sub>2</sub>O was influenced positively by NO<sub>3</sub><sup>-</sup> in the Leybeek pond and by NH<sub>4</sub><sup>+</sup> in the Pêcherie and Tenreuken ponds (Table S8). %N<sub>2</sub>O was influenced positively by Chl-*a* and TSM in the Tenreuken pond, and negatively by Chl-*a* in the Leybeek pond (Table

321 S5), probably reflecting the negative influence on Chl-*a* and TSM by  $T_w$  in the Tenreuken pond and the positive influence  
322 on Chl-*a* by  $T_w$  in the Leybeek pond (Table S6).

### 323 3.2. Drivers of bubble flux

324 The bubble flux measured with inverted funnels in the four sampled ponds in the city of Brussels ranged between 0 and 2078  
325  $\text{ml m}^{-2} \text{d}^{-1}$  and was influenced positively by  $T_w$  in all four systems (Fig. 4). The mean  $\text{CH}_4$  content of the bubbles in the four  
326 sampled ponds in the city of Brussels was  $31 \pm 21\%$ , and values were influenced positively by  $T_w$  in the Silex pond (Fig. 4).  
327 The  $\text{CH}_4$  content of the bubbles was correlated with bubble flux (Fig. S3) as both variables were positively influenced by  $T_w$   
328 (Fig. 4).

329 The time-series at the Silex pond allowed investigating in more detail the effects of  $T_w$  and atmospheric pressure variations  
330 on bubble fluxes (Fig. 5). In spring 2022, the bubble flux at the Silex pond increased during drops in atmospheric pressure  
331 (depressions) (Fig. 5). There was no relation between wind speed and peaks of bubble flux ( $r^2 = 0.01$ ,  $p = 0.463$ ), suggesting a  
332 more important role of changes of atmospheric pressure than of wind speed in triggering bubble fluxes in the Silex pond in  
333 spring 2022. The bubble flux at the Silex pond was higher in summer ( $1152 \pm 433 \text{ mL m}^{-2} \text{d}^{-1}$ ) than during spring ( $198 \pm 170$   
334  $\text{mL m}^{-2} \text{d}^{-1}$ ) and the temporal changes of bubble fluxes tracked those of  $T_w$  (Fig. 5). In order to evaluate the relative  
335 importance of changes of atmospheric pressure and water temperature in triggering bubble fluxes, the bubble flux was  
336 modelled as function of  $T_w$  alone or as function of both  $T_w$  and  $\Delta p$  (Figs. 5, S4). For periods of low  $T_w$  ( $< 15^\circ\text{C}$ ), the  
337 inclusion of the term of  $\Delta p$  in the model improved the performance of the model by comparison to the measurements (Figs.  
338 5, S4). But for warmer periods ( $> 15^\circ\text{C}$ ), when bubbling fluxes were quantitatively more important, the inclusion in the  
339 model of the term of  $\Delta p$  did not improve the performance of the model (Figs. 5, S4). For the full  $T_w$  range ( $< 15^\circ\text{C}$  and  
340  $> 15^\circ\text{C}$ ), the inclusion of the term of  $\Delta p$  only improved the performance of the model very marginally (Fig. S4).

### 341 3.3. Drivers of methane ebullitive fluxes

342 Ebullitive  $\text{CH}_4$  fluxes in the four ponds ranged between 0 and  $59 \text{ mmol m}^{-2} \text{d}^{-1}$  and were positively related to  $T_w$  (Fig. 6).  
343 The fitted relations between ebullitive  $\text{CH}_4$  fluxes and  $T_w$  were specific to each pond and encompassed the fitted relations  
344 established in similar systems: four small ponds in Québec (DelSontro et al., 2016) and a small urban pond in the  
345 Netherlands (Aben et al., 2017). The  $Q_{10}$  of  $\text{CH}_4$  ebullition values ranged between 4.4 in the deeper Pêcherries pond and 26.9  
346 in the shallower Leybeek pond (Table S9). The  $Q_{10}$  of  $\text{CH}_4$  ebullition in the four studied ponds of the city of Brussels, in  
347 Québec (DelSontro et al., 2016), and in the Netherlands (Aben et al., 2017) were negatively related to water depth (Fig. 6).

### 348 3.4. Relative contribution of methane ebullitive and diffusive fluxes

349 Diffusive  $\text{CH}_4$  fluxes computed from dissolved  $\text{CH}_4$  concentration and  $k$  derived from wind speed ranged between 0.1 and  
350  $19.7 \text{ mmol m}^{-2} \text{d}^{-1}$  (Fig. 7). The diffusive  $\text{CH}_4$  fluxes tended to be higher in summer and spring than in fall and winter owing  
351 to the strong positive influence on  $\text{CH}_4$  dissolved concentration by  $T_w$  (Fig. 3; Tables S4, S5). In addition, wind speed only  
352 showed small seasonal variations during sampling ( $0.6 \pm 0.6 \text{ m s}^{-1}$  in spring,  $0.3 \pm 0.2 \text{ m s}^{-1}$  in summer,  $0.7 \pm 0.7 \text{ m s}^{-1}$  in fall, and  
353  $0.6 \pm 0.2 \text{ m s}^{-1}$  in winter) (Fig. S2). Ebullitive  $\text{CH}_4$  fluxes were calculated from the relations with  $T_w$  for each pond given in  
354 Figure 6 from the  $T_w$  data coincident with the diffusive  $\text{CH}_4$  fluxes (Fig. 7). The resulting calculated ebullitive  $\text{CH}_4$  fluxes  
355 allowed to compare and integrate seasonally both components of  $\text{CH}_4$  emissions to the atmosphere, and to calculate the  
356 relative contribution of ebullition to total (diffusive+ebullitive)  $\text{CH}_4$  emissions. The relative contribution of ebullition to total  
357  $\text{CH}_4$  emissions ranged between 1 and 99% in the four sampled ponds in the city of Brussels (Fig. 7) and was influenced

positively by  $T_w$  (Fig. S5). The values of  $Q_{10}$  of diffusive  $CH_4$  fluxes were lower than those for ebullitive  $CH_4$  fluxes in each pond, and less variable (1.2 in the Pêcherries pond to 2.9 in the Silex pond) (Table S9).

The annually averaged diffusive and ebullitive fluxes of  $CH_4$  in the four ponds in the city of Brussels were plotted against annually averaged Chl-*a* concentration, total macrophyte cover in summer, water depth, and lake surface area (Fig. 8) that are frequent predictors of variations of  $CH_4$  fluxes among lakes (Holgerson and Raymond, 2016; DelSontro et al., 2018, Deemer and Holgerson, 2021; Casas-Ruiz et al., 2021; Borges et al., 2022). The annually averaged ebullitive  $CH_4$  fluxes were significantly higher in the two clear-water ponds ( $7.3 \pm 2.9$  and  $13.4 \pm 3.7$  mmol  $m^{-2} d^{-1}$  in the Tenreuken and the Silex ponds, respectively) than the two turbid-water ponds ( $3.8 \pm 3.2$  and  $2.5 \pm 1.4$  mmol  $m^{-2} d^{-1}$  in the Leybeek and the Pêcherries ponds, respectively) (Table S7). The annually averaged ebullitive  $CH_4$  fluxes were significantly higher in the Silex pond, that showed a higher macrophyte cover during summer (100% in the Silex pond and 68% in the Tenreuken pond), than the Tenreuken pond ( $p < 0.0001$ , Table S7) and were not significantly different in the two turbid-water Leybeek and Pêcherries ponds ( $p = 0.0617$ , Table S7) that showed similar macrophyte cover during summer (6 and 9% in the Leybeek and Pêcherries ponds, respectively) (Fig. 8). The annually averaged ebullitive  $CH_4$  fluxes were overall influenced positively by macrophyte cover and negatively by Chl-*a* (Fig. 8).

In the four sampled urban ponds, annually averaged  $CH_4$  diffusive fluxes were higher in the pond with the highest total macrophyte cover in the clear-water ponds, and higher in the pond with the highest Chl-*a* concentration in the turbid-water ponds (Fig. 8). The annually averaged relative contribution of ebullition to total  $CH_4$  emissions were higher in the two clear-water ponds than the two turbid-water ponds (Table S7). The relative contribution of ebullitive  $CH_4$  fluxes to the total  $CH_4$  flux was influenced positively by macrophyte cover and negatively by Chl-*a* (Fig. 8).

The annually averaged diffusive fluxes of  $CO_2$  ( $F_{CO_2}$ ) and  $N_2O$  ( $F_{N_2O}$ ) in the four ponds in the city of Brussels were also plotted against annually averaged Chl-*a* concentration, total macrophyte cover in summer, water depth, and lake surface area (Fig. S6). Annually averaged  $F_{CO_2}$  were lower in the Leybeek pond than the Pêcherries and the Silex ponds (Table S7).  $F_{CO_2}$  was not significantly influenced by the other variables (Chl-*a* concentration, total macrophyte cover, water depth, and lake surface area) (Fig. S6). Annually averaged  $F_{N_2O}$  was not significantly different between clear-water and turbid-water ponds.  $F_{N_2O}$  was significantly lower in the deeper Pêcherries pond than the two shallower Leybeek and Silex ponds (Table S7), and  $F_{N_2O}$  showed a significant negative relationship with water depth (Fig. S6).

### 3.5. Relative contribution of $CO_2$ , $CH_4$ and $N_2O$ emissions

The emissions in  $CO_2$ -eq for the 3 GHGs averaged per season for both 2022 and 2023 peaked seasonally in summer in the Silex ( $2.9$  mg  $CO_2$ -eq  $m^{-2} d^{-1}$ ), the Tenreuken ( $1.7$  mg  $CO_2$ -eq  $m^{-2} d^{-1}$ ), and the Leybeek ( $1.1$  mg  $CO_2$ -eq  $m^{-2} d^{-1}$ ) pond (Fig. 9), but peaked in fall in the Pêcherries pond ( $1.3$  mg  $CO_2$ -eq  $m^{-2} d^{-1}$ ). The higher value of the total GHG emissions in fall compared to other seasons in the Pêcherries pond was due to an increase of  $CO_2$  emissions in fall that surpassed the peak of  $CH_4$  emissions in summer. The GHG fluxes were lowest in winter in the Silex ( $1.3$  mg  $CO_2$ -eq  $m^{-2} d^{-1}$ ), the Tenreuken ( $0.9$  mg  $CO_2$ -eq  $m^{-2} d^{-1}$ ), the Pêcherries ( $0.8$  mg  $CO_2$ -eq  $m^{-2} d^{-1}$ ), and the Leybeek ( $0.6$  mg  $CO_2$ -eq  $m^{-2} d^{-1}$ ) ponds. The relative contribution of ebullitive  $CH_4$  fluxes peaked in summer in the Silex (73.8%), the Tenreuken (70.9%), the Pêcherries (23.6%), and the Leybeek (58.3%) ponds. The relative contribution of ebullitive  $CH_4$  fluxes was lowest in winter in the Silex (22.1%), the Tenreuken (10.0%), the Pêcherries (6.7%), and the Leybeek (1.0%) ponds.

The annual emissions in  $CO_2$ -eq of the three GHGs ( $CO_2$ ,  $CH_4$ , and  $N_2O$ ) in 2022 and 2023 were higher in the two clear-water ponds ( $1.3 \pm 0.5$  and  $1.8 \pm 0.9$  mg  $CO_2$ -eq  $m^{-2} d^{-1}$  in the Tenreuken and Silex ponds, respectively) than in the two turbid-

396 water ponds ( $1.0 \pm 0.2$  and  $0.9 \pm 0.5$  mg CO<sub>2</sub>-eq m<sup>-2</sup> d<sup>-1</sup> in the Leybeek and Pêcherries ponds, respectively) (Fig. 9) due to higher  
 397 total CH<sub>4</sub> emissions (diffusive+ebullitive) in clear-water ponds ( $0.7 \pm 0.4$  and  $1.2 \pm 0.5$  mg CO<sub>2</sub>-eq m<sup>-2</sup> d<sup>-1</sup> in the Tenreuken and  
 398 Silex ponds, respectively) than in turbid-water ponds ( $0.2 \pm 0.2$  and  $0.4 \pm 0.3$  mg CO<sub>2</sub>-eq m<sup>-2</sup> d<sup>-1</sup> in the Leybeek and Pêcherries  
 399 ponds, respectively). The contribution of N<sub>2</sub>O to the total GHG emissions was marginal and did not affect the differences in  
 400 total GHG fluxes between ponds, with the highest contribution observed in the Leybeek pond, with a contribution of 1.7%.

401 The majority of GHG emissions in CO<sub>2</sub>-eq was related to CO<sub>2</sub> and CH<sub>4</sub> (diffusive+ebullitive) in the four ponds. In turbid-  
 402 water ponds CO<sub>2</sub> represented the largest fraction of GHG emissions (68.5% (2022) and 79.3% (2023) in the Pêcherries pond,  
 403 and 49.0% (2022) and 58.3% (2023) in the Leybeek pond). In clear-water ponds CH<sub>4</sub> represented the largest fraction of  
 404 GHG emissions (66.5% (2022) and 63.3% (2023) in the Silex pond, and 60.8% (2022) and 50.0% (2023) in the Tenreuken  
 405 pond). The higher annual GHG emissions in CO<sub>2</sub>-eq from the two clear-water ponds than the turbid-water ponds were  
 406 related to the higher contribution of ebullitive CH<sub>4</sub> fluxes.

407 The annual GHG fluxes increased from 2022 to 2023 due to an increase in relative contribution of CO<sub>2</sub> diffusive emissions  
 408 in all four ponds. Diffusive CO<sub>2</sub> emissions averaged annually in all four ponds 0.5 mg CO<sub>2</sub> m<sup>-2</sup> d<sup>-1</sup> in 2022 and 0.7 mg CO<sub>2</sub>  
 409 m<sup>-2</sup> d<sup>-1</sup> in 2023. Diffusive CO<sub>2</sub> emissions were 2.1 times higher in summer 2023 than in summer 2022, and 2.5 times higher  
 410 in fall 2023 than in fall 2022, and showed similar values between 2023 and 2022 in spring and winter (1.1 higher and 1.1  
 411 lower, respectively).

#### 412 4. Discussion

413 The Leybeek and Pêcherries ponds are turbid-water systems (high Chl-*a* and TSM values, low submerged macrophyte cover)  
 414 and the Tenreuken and Silex ponds are clear-water systems (low Chl-*a* and TSM values, high submerged macrophyte cover)  
 415 (Figs. 1, 3). All four ponds have a relatively similar size (0.7 to 3.2 ha) and depth (0.5 to 1.4 m) and are uniformly located in  
 416 an urban landscape in the city of Brussels. It can be assumed that, among the four systems, the major difference that is  
 417 expected to affect GHG emissions is the dominance of aquatic primary producer, either phytoplankton or macrophytes,  
 418 corresponding to two alternative states *sensu* Scheffer et al. (1993). Our data-set provides the opportunity to investigate the  
 419 effect of the two alternative states on GHG emissions from small lentic systems.

420 The reported pCO<sub>2</sub> values (40 to 13,804 ppm) (Fig. 3) in the four ponds in the city of Brussels were within the range of  
 421 values typically observed in ponds (Holgerson and Raymond, 2016; Peacock et al., 2019; Audet et al., 2020) (Fig. 3). The  
 422 pCO<sub>2</sub> values were influenced negatively by %O<sub>2</sub> and positively by DIN and SRP across seasons (Tables S4, S5) showing  
 423 that their seasonal variability was driven by aquatic primary production and degradation of organic matter (*e.g.* Holgerson  
 424 2015). Accordingly, low values of pCO<sub>2</sub> were generally observed in spring and summer probably due to uptake of CO<sub>2</sub> by  
 425 primary production from either phytoplankton or submerged macrophytes. High values of pCO<sub>2</sub> were observed in fall in the  
 426 four ponds and probably reflect the release of CO<sub>2</sub> from degradation of organic matter due to the senescence of  
 427 phytoplankton or macrophytes (Fig. 3). In all four ponds, pCO<sub>2</sub> values were influenced positively by precipitation (Tables  
 428 S4, S5) suggesting an additional control of external inputs of carbon either as organic carbon sustaining internal degradation  
 429 of organic matter or as soil CO<sub>2</sub> (*e.g.* Marotta et al., 2010; Ojala et al., 2011; Rasilo et al., 2012; Vachon and del Giorgio,  
 430 2014; Holgerson, 2015). The %N<sub>2</sub>O values (32 to 826%) (Fig. 3) in the four ponds were within the range of values typically  
 431 observed in ponds (Audet et al., 2020; Rabaey and Cotner, 2022). When all the data were pooled, the %N<sub>2</sub>O was influenced  
 432 positively by DIN (Table S4) as also frequently reported by other studies in ponds and interpreted as a control of nitrification  
 433 and/or denitrification (hence N<sub>2</sub>O production) by DIN levels (Audet et al., 2020; Webb et al., 2021; Wang et al., 2021; Xie

et al., 2024). The negative influence on %N<sub>2</sub>O by T<sub>w</sub> (Table S4) might reflect the effect of the inhibition at low temperatures of the final step of denitrification leading to an accumulation of N<sub>2</sub>O (Velthuis and Veraart, 2022) but could also indirectly result from the higher DIN values observed at low T<sub>w</sub> values (Table S6). The CH<sub>4</sub> dissolved concentrations (194 to 48,380 nmol L<sup>-1</sup>) (Fig. 3) in the four ponds were within the range of values typically observed in ponds (Natchimuthu et al., 2014; Holgerson and Raymond, 2016; Peacock et al., 2019; Audet et al., 2020; Rabaey and Cotner, 2022; Ray et al., 2023), and were influenced positively by T<sub>w</sub> in all four ponds individually and when pooled (Tables S4, S5), most probably reflecting the increase of sedimentary methanogenesis with temperature (Schulz and Conrad, 1996).

Temperature also exerted a strong control on bubble flux from sediments and ebullitive CH<sub>4</sub> emissions. The bubble flux values (0 and 2078 ml m<sup>-2</sup> d<sup>-1</sup>) in the four sampled ponds (Fig. 4) were within the range of values reported in lentic systems of equivalent size by Wik et al. (2013) (0 to 2772 mL m<sup>-2</sup> d<sup>-1</sup>), DelSontro et al. (2016) (11 to 748 mL m<sup>-2</sup> d<sup>-1</sup>), and Ray and Holgerson (2023) (0 to 2079 mL m<sup>-2</sup> d<sup>-1</sup>). The bubble flux was influenced positively by T<sub>w</sub> (Fig. 4) in agreement with previous studies (*e.g.* Wik et al., 2013; DelSontro et al., 2016; Aben et al., 2017; Ray and Holgerson, 2023). Bubbling events from lake sediments are known to also be triggered by a decrease of hydrostatic pressure on the sediments due to water level fluctuations or drops in atmospheric pressure (Tokida et al., 2007; Scandella et al., 2011; Varadharajan and Hemond, 2012; Wik et al., 2013; Taoka et al., 2020; Zhao et al., 2021). In the Silex pond, in spring 2022, some peaks in bubble fluxes were related to drops in atmospheric pressure (Fig. 5) but unrelated to wind speed as shown in Gatun Lake (Keller and Stallard, 1994). A statistical model of the bubble flux that included the contributions of T<sub>w</sub> and  $\Delta p$  was used to quantify the relative importance of each of these two drivers (Fig. S4) and showed that air pressure drop seemed quantitatively important only at low T<sub>w</sub> and that the intensity of bubble flux was mainly driven by temperature change at yearly scales, in agreement with previous studies (*e.g.* Wik et al., 2013; DelSontro et al., 2016; Aben et al., 2017; Ray and Holgerson, 2023).

The mean CH<sub>4</sub> content of the bubbles (31±21%) in the four sampled ponds in the city of Brussels was comparable to the values obtained by Wik et al. (2013) (35±25%), DelSontro et al. (2016) (58±25%), and Ray and Holgerson (2023) (25±13%) in lentic systems of similar size. The increasing pattern of the CH<sub>4</sub> content of the bubbles with T<sub>w</sub> (Fig. 4) was most probably related to the strong dependence of methanogenesis on temperature (Schulz and Conrad, 1996). The increase of methanogenesis with temperature leads to the build-up of gas bubbles in sediments that are richer in CH<sub>4</sub>, and consequently to higher bubble fluxes with a higher CH<sub>4</sub> content at higher temperatures (Figs. 4, S3). Since both bubble flux and the CH<sub>4</sub> content of the bubbles increased with T<sub>w</sub> (Fig. 4), the ebullitive CH<sub>4</sub> fluxes in the four ponds were also positively related to T<sub>w</sub> (Fig. 6) as shown previously in other small lentic systems (*e.g.* Wik et al., 2013; DelSontro et al., 2016; Natchimuthu et al., 2016; Aben et al., 2017; Ray and Holgerson, 2023; Rabaey and Cotner, 2024). Yet, the dependency of CH<sub>4</sub> ebullition on temperature (Q<sub>10</sub>) was different among the four ponds and was negatively related to depth including data from systems in Québec (DelSontro et al., 2016) and The Netherlands (Aben et al., 2017) (Fig. 6). This implies that an increase in T<sub>w</sub> leads to a smaller increase in CH<sub>4</sub> ebullitive fluxes (lower Q<sub>10</sub>) in deeper ponds as the impact of hydrostatic pressure on sediments is higher in deeper ponds compared to shallow ponds, restricting bubble formation and release (*e.g.* DelSontro et al., 2016). This dependence of Q<sub>10</sub> of CH<sub>4</sub> ebullition to depth suggests that the response of CH<sub>4</sub> ebullition to heatwaves (or longer-term warming) might be more intense the shallower the pond, in addition to other effects from heat-waves on GHG emissions (*e.g.* Audet et al., 2017).

The values of Q<sub>10</sub> for diffusive CH<sub>4</sub> fluxes in the four ponds were lower than those for ebullitive CH<sub>4</sub> fluxes (Table S9) as reported by other studies in lentic systems (DelSontro et al., 2016; Xun et al., 2024). The lower dependence to T<sub>w</sub> of diffusive CH<sub>4</sub> fluxes compared to ebullitive CH<sub>4</sub> fluxes might be related to a lower relative change of CH<sub>4</sub> concentrations

473 and  $k$  with the variation of  $T_w$ . Dissolved  $CH_4$  concentrations in surface waters of lentic systems are strongly affected by  
474 microbial methane oxidation (*e.g.* Bastviken et al., 2002). A relative increase of methanogenesis in sediments might lead to a  
475 stronger increase of  $CH_4$  emission by ebullition than by diffusion because of a reduction of  $CH_4$  diffusive emissions resulting  
476 from methane oxidation. Additionally,  $k$  depends on wind speed, but in the four ponds, the warmer periods of the year  
477 (summer) tended to be less windy ( $\sim 0.3 \text{ m s}^{-1}$ ) than the other seasons ( $> 0.6 \text{ m s}^{-1}$ ) also contributing to a lower dependence on  
478  $T_w$  of  $CH_4$  diffusive fluxes compared to ebullitive fluxes and lower  $Q_{10}$  values.

479 The difference in the  $Q_{10}$  of diffusive and ebullitive  $CH_4$  fluxes was consistent with a variable contribution of the diffusive  
480 and ebullitive  $CH_4$  fluxes seasonally as a function of  $T_w$ , with the contribution of ebullitive  $CH_4$  fluxes strongly increasing  
481 with  $T_w$  in the four ponds (Fig. S5). At annual scale, ebullitive  $CH_4$  fluxes represented between 55% and 83% of the total  
482  $CH_4$  emissions in the Leybeek and Silex ponds, respectively. This finding is consistent with other studies showing that  
483 ebullitive  $CH_4$  fluxes can account for more than half of total  $CH_4$  emissions in small and shallow lentic systems (*e.g.* Wik et  
484 al., 2013; Deemer and Holgerson, 2021; Ray and Holgerson, 2023; Rabaey and Cotner, 2024). The averaged ebullitive  $CH_4$   
485 emissions were higher in the two clear-water ponds ( $10.4 \text{ mmol m}^{-2} \text{ d}^{-1}$ ) than the two turbid-water ponds ( $3.2 \text{ mmol m}^{-2} \text{ d}^{-1}$ )  
486 (Fig. 7). The averaged ebullitive  $CH_4$  emissions in the four ponds were influenced positively by macrophyte cover and  
487 negatively by  $Chl-a$  (Fig. 8). The higher ebullitive  $CH_4$  emissions from the two clear-water ponds would suggest that the  
488 delivery of organic matter to sediments from macrophytes sustained a quantitatively larger methane production than from  
489 phytoplankton. This finding is consistent with the notion that vegetated littoral zones of lakes are hot spots of  $CH_4$   
490 production and emission (*e.g.* Hyvönen et al., 1998; Huttunen et al., 2003; Juutinen et al., 2003; Desrosiers et al., 2022).  $CH_4$   
491 fluxes in lentic systems have been extrapolated at globally scale assuming a dependency on aquatic productivity using  $Chl-a$   
492 as a predictor (*e.g.* DelSontro et al., 2018). The negative relation between  $CH_4$  ebullitive fluxes with  $Chl-a$  shows that  $Chl-a$   
493 concentration alone fails to predict ebullitive fluxes in macrophyte-dominated clear-water ponds.

494 The annually averaged diffusive  $CH_4$  emissions in the four ponds seemed to respond positively to both increasing  
495 phytoplankton and macrophyte biomass resulting in a U-shaped relation between diffusive  $CH_4$  emissions and  $Chl-a$  as well  
496 as macrophyte cover (Fig. 8). Higher values of annually averaged  $CH_4$  diffusive fluxes occurred at the extreme values of  
497  $Chl-a$  or of macrophyte cover (minimum or maximum), and lower values occurred at the intermediate values of  $Chl-a$  or  
498 macrophyte cover. Such U-shape relation resulted from the inverse relationship between macrophyte cover and  $Chl-a$   
499 (alternative states) and is consistent with reported positive relation between diffusive  $CH_4$  fluxes with both macrophyte cover  
500 (*e.g.* Ray et al., 2023; Theus et al., 2023) as well as with phytoplankton biomass (*e.g.* DelSontro et al., 2018; Yan et al.,  
501 2019; Bartosiewicz et al., 2021). The relative contribution of ebullitive  $CH_4$  fluxes to the total annual  $CH_4$  flux increased  
502 with the macrophyte cover (Fig. 8), in agreement with the idea of an increase of  $CH_4$  ebullition relative to diffusive  $CH_4$   
503 emissions in vegetated sediments compared to unvegetated sediments (*e.g.* Desrosiers et al., 2022; Ray et al., 2023; Theus et  
504 al., 2023).

505 Fluxes of  $CH_4$  and  $CO_2$  have been reported to be negatively related to surface area and depth by numerous studies in ponds  
506 (*e.g.* Holgerson, 2015; Holgerson and Raymond, 2016; Ray et al., 2023; Theus et al., 2023) and lakes (*e.g.* Kankaala et al.,  
507 2013; DelSontro et al., 2018, Deemer and Holgerson, 2021; Casas-Ruiz et al., 2021; Borges et al., 2022). Annual diffusive  
508  $F_{CH_4}$  and  $F_{CO_2}$  were both unrelated to surface area and depth in the four studied ponds (Figs. 8, S6) resulting from the narrow  
509 range of variation of water depth (0.6 to 1.4 m) and surface area (0.7 to 3.2 ha). The lack of relationship between annual  $F_{CO_2}$   
510 and both  $Chl-a$  and macrophyte cover in the four ponds (Fig. S6) might be surprising since other studies have reported lower  
511  $CO_2$  fluxes in more productive lentic systems (*e.g.* Sand-Jensen and Staehr, 2007; Borges et al., 2022). We hypothesize that

512 given that the four systems were either phytoplankton-dominated or macrophyte-dominated (alternative states), the ponds  
513 had an important submerged productivity, in both cases, resulting in a relatively invariant  $F_{CO_2}$  as function of either Chl-*a* or  
514 macrophyte cover.

515 Global average emissions of GHGs in  $CO_2$ -eq from inland waters are dominated by  $CO_2$  followed by  $CH_4$  with a small  
516 contribution from  $N_2O$  according to Lauerwald et al. (2023). However, in small lentic systems such as ponds, the  $CO_2$ -eq  
517 emissions from  $CH_4$  can match or dominate those of  $CO_2$  (e.g. Webb et al., 2023; Ray and Holgerson, 2023; Rabaey and  
518 Cotner, 2024). The meta-analysis of Holgerson and Raymond (2016) suggested that the  $CO_2$  and  $CH_4$  emissions in  $CO_2$ -eq  
519 are numerically close in small lentic systems such as ponds but become increasingly dominated by  $CO_2$  emissions in larger  
520 lentic systems. In the four studied ponds, the GHG emissions in  $CO_2$ -eq were dominated by  $CO_2$  and  $CH_4$  with a marginal  
521 contribution (<1%) from  $N_2O$  (Fig. 9). Annually,  $CO_2$  represented the largest fraction of GHG emissions in  $CO_2$ -eq (~60%)  
522 in turbid-water ponds (Leybeek and Pêcheres), while  $CH_4$  represented the largest fraction of GHG emissions in  $CO_2$ -eq  
523 (~60%) in clear-water ponds (Silex and Tenreuken) as a result of higher ebullitive  $CH_4$  fluxes in the clear-water ponds (Fig.  
524 7).

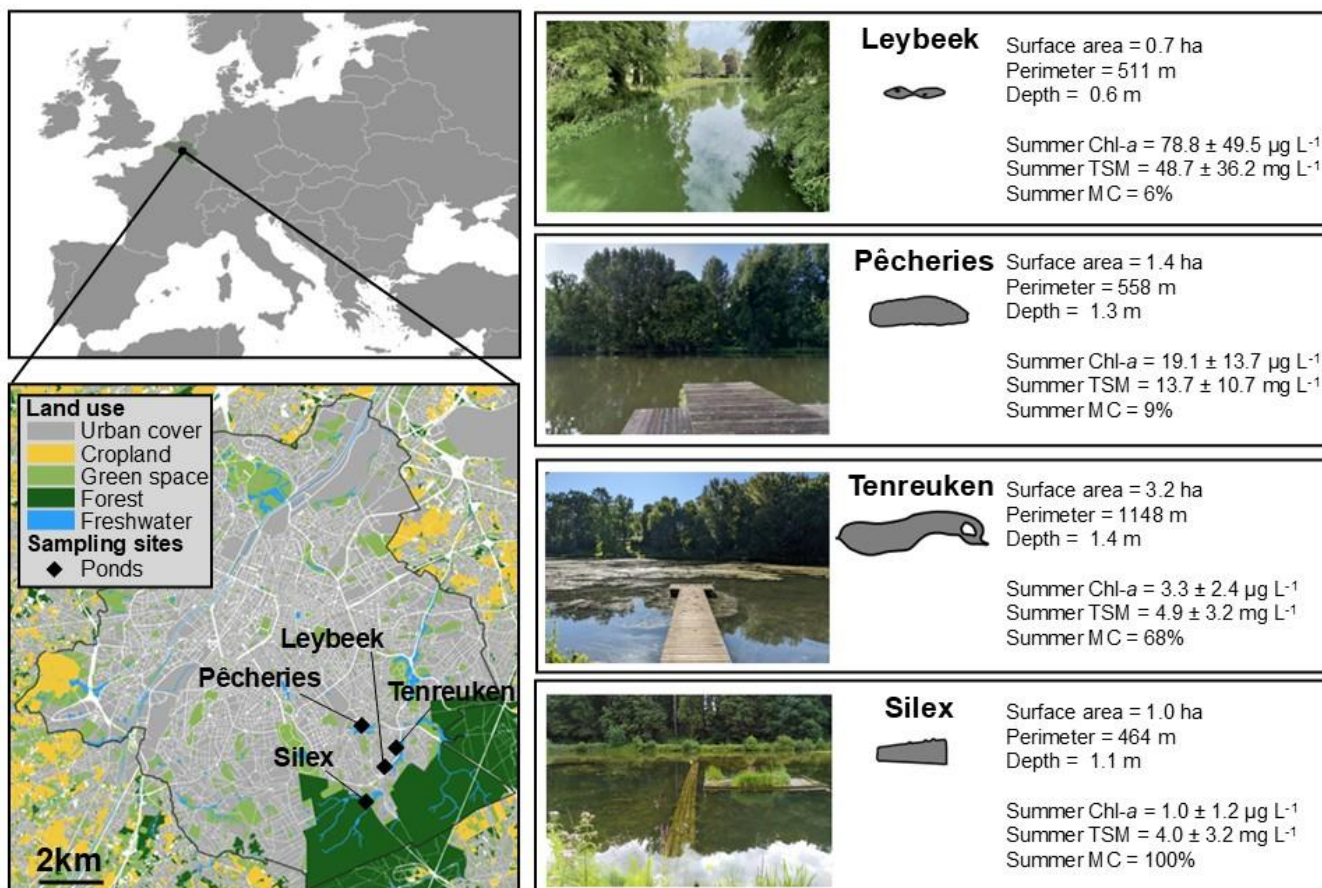
525 The annual GHG emissions in  $CO_2$ -eq increased from 2022 to 2023 due to an increase in the relative contribution of  $CO_2$   
526 diffusive emissions in all four ponds (Fig. 9) as a result of higher precipitation in 2023 (Fig. 2). Air temperatures were  
527 similar in both years (annual average of 12.2°C in 2022 and 12.1°C in 2023), and precipitation was 1.5 times higher in 2023  
528 than in 2022. Higher precipitation is likely to increase the inputs of organic and inorganic carbon from soils to ponds, as  
529 previously shown in other lentic systems (e.g. Marotta et al., 2011; Ojala et al., 2011; Rasilo et al., 2012; Vachon and del  
530 Giorgio, 2014; Holgerson, 2015). This hypothesis is only based on the comparison of two years but the increase of the  
531 relative contribution of  $CO_2$  diffusive emissions in 2023 was observed in all four ponds. The synchronicity of the increase of  
532  $CO_2$  diffusive emissions in 2023 compared to 2022 suggests a common uniform driver in all four ponds that would be  
533 consistent with a large variation in weather between the two years such as annual precipitation. The El Niño event in 2023  
534 induced low-level cyclonic wind anomalies and higher precipitation over Western Europe, including Belgium (Chen et al.,  
535 2024).

## 536 5. Conclusions

537 Ebullitive  $CH_4$  emissions in 2022-2023 were higher in the two clear-water, macrophyte-dominated ponds (Tenreuken and  
538 Silex) than in the two turbid-water, phytoplankton-dominated ponds (Pêcheres and Leybeek) of the city of Brussels,  
539 although, the diffusive  $CH_4$  fluxes were not systematically significantly different between the clear-water ponds and the  
540 turbid-water ponds. The annually averaged diffusive  $N_2O$  and  $CO_2$  fluxes were not significantly different in the two clear-  
541 water ponds from those in the two turbid-water ponds. Other studies have found no difference in  $N_2O$  sedimentary  
542 production in lakes with high and low density of submerged macrophytes. We hypothesize that  $CO_2$  fluxes were relatively  
543 invariant among the four sampled ponds because of their similar size, depth, and putatively productivity (either from  
544 phytoplankton or submerged macrophytes). The total (diffusive and ebullitive)  $CH_4$  emissions represented 58% of total  
545 annual GHG emissions in  $CO_2$ -eq in the two clear-water ponds compared to 41% in the two turbid-water ponds.  $CO_2$   
546 represented nearly all the remainder of total annual GHG emissions in  $CO_2$ -eq, and  $N_2O$  represented a very marginal fraction  
547 (<2%).

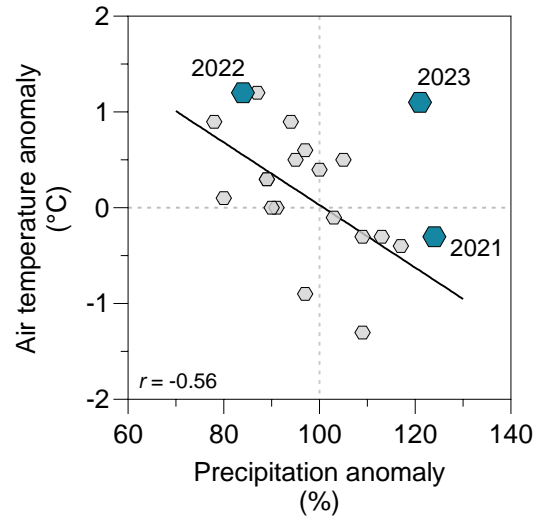
548 The seasonal variations of GHG emissions were mainly driven by  $CH_4$  ebullitive emissions that peaked in summer (both  
549 quantitatively and relatively), as  $CH_4$  ebullition was related positively to  $T_w$  resulting from an increase in both flux of

550 bubbles and CH<sub>4</sub> content of bubbles with warming. The pCO<sub>2</sub> values in the four sampled ponds increased with precipitation  
551 at seasonal scale, probably in relation to higher inputs of organic and inorganic carbon from soils . Years 2022 and 2023  
552 were abnormally dry and wet, respectively, and the GHG emissions were higher in 2023 mainly due to an increase in the  
553 relative contribution of CO<sub>2</sub> emissions, probably in response to a strong El Niño event. This would suggest that variations of  
554 precipitation also affected year-to-year variations of CO<sub>2</sub> emissions in addition to partly regulating seasonal variations of  
555 CO<sub>2</sub> emissions from the four studied ponds.



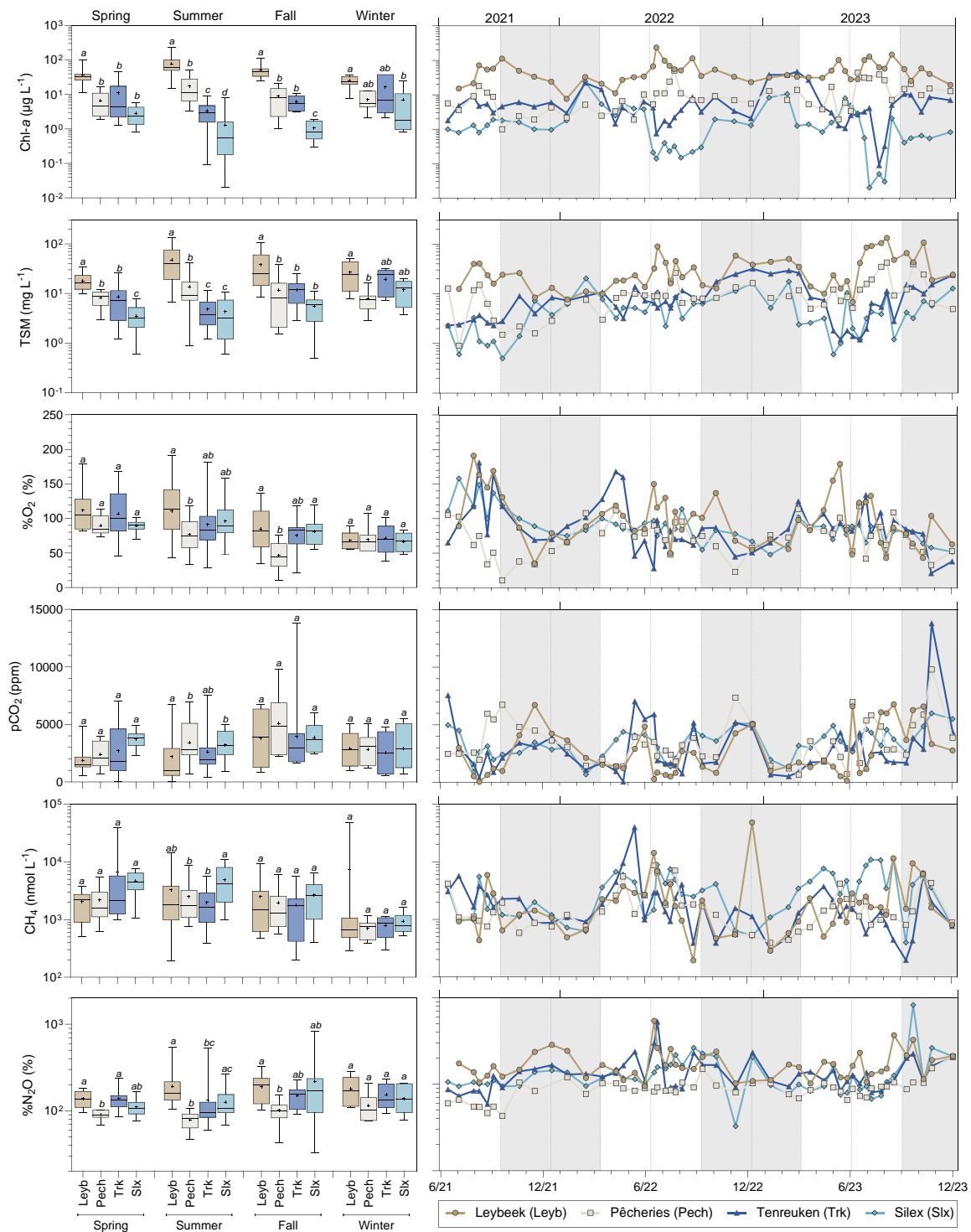
556

557 Figure 1: Location of the four sampled urban ponds (black diamonds) in city of Brussels (Belgium) delineated by the black line.  
 558 Right panels indicate for each pond the shape of the ponds, surface area (ha), perimeter (m), average depth (m), mean±standard  
 559 deviation of chlorophyll-*a* (Chl-*a*, in  $\mu\text{g L}^{-1}$ ) and total suspended matter (TSM, in  $\text{mg L}^{-1}$ ) in summer (21 June to 21 September in  
 560 2021, 2022, 2023), and summer total macrophyte cover (MC, in %) (Table S1).



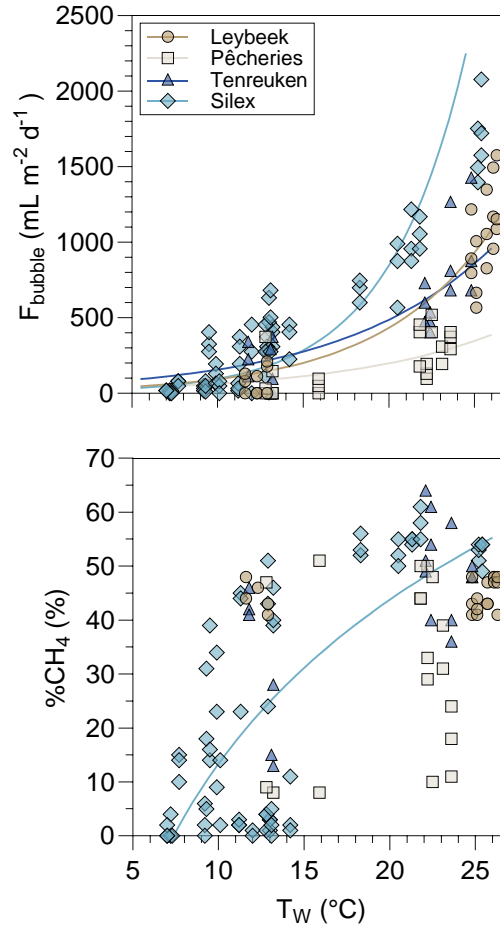
561

562 **Figure 2: Anomaly of annual air temperature (°C) as a function of anomaly of annual precipitation (%) from 2003 to 2023 with**  
563 **respect to average of the 1991-2020 period (11 °C and 837 mm, respectively). Small grey hexagons represent anomaly values for**  
564 **years 2003-2020 and larger blue hexagons represent anomaly values for years 2021-2023. The solid line shows the linear**  
565 **correlation of air temperature anomaly as a function of precipitation anomaly for years 2003-2020 ( $Y = 3.29 - 0.0327 \cdot X$ ,**  
566  **$n=20$ ) and  $r$  denotes the Pearson correlation coefficient. Note the anomalous rainy year in 2023 relative to the pattern of**  
567 **precipitation as function of temperature anomalies for the other years, possibly in response to the strong El Niño event of 2023**  
568 **(Chen et al., 2024).**



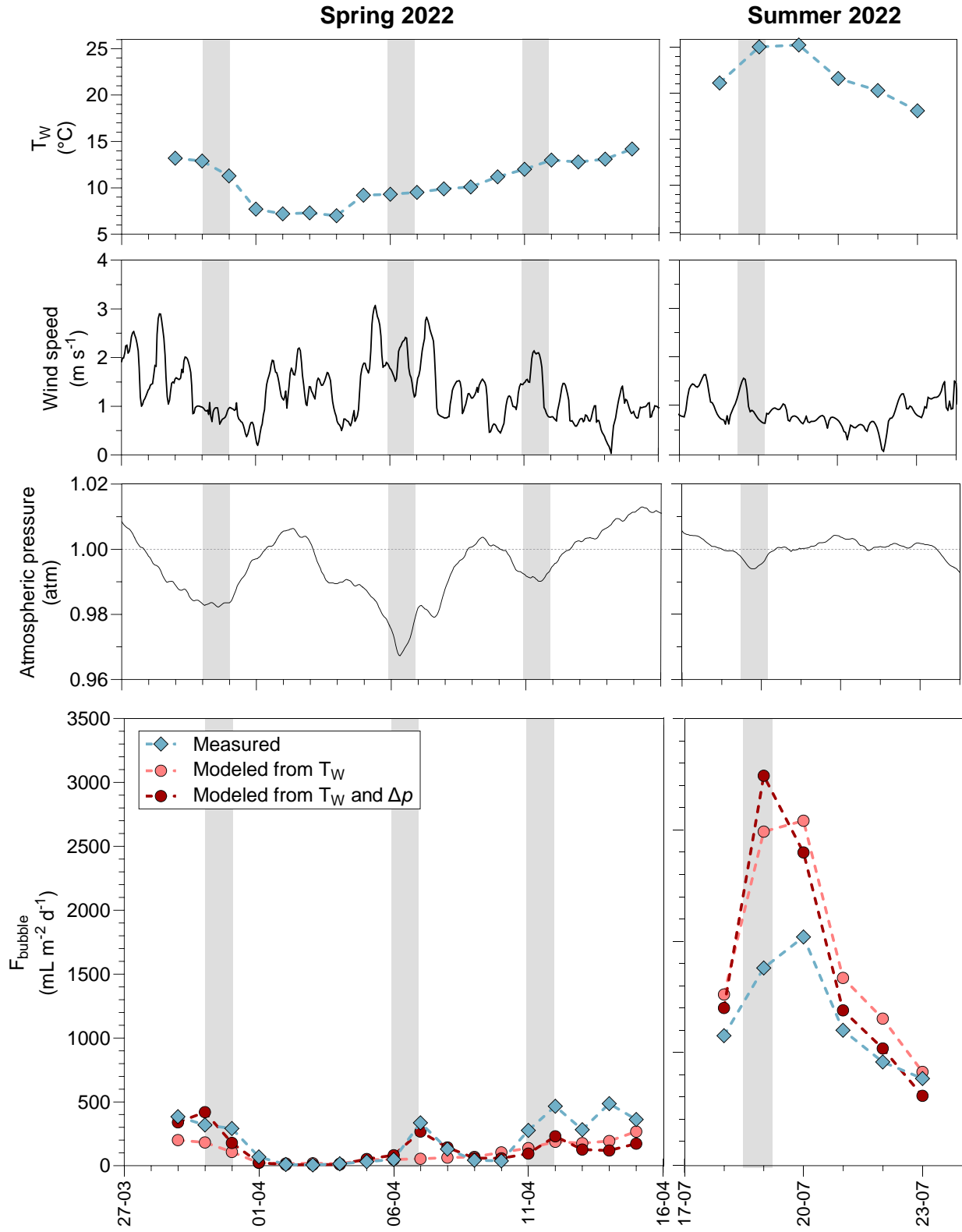
569

570 **Figure 3: Seasonal variations of Chlorophyll-a (Chl-a, in  $\mu\text{g L}^{-1}$ ), total suspended matter (TSM, in  $\text{mg L}^{-1}$ ), oxygen saturation**  
 571 **( $\%O_2$ , in  $\%$ ), partial pressure of  $CO_2$  ( $pCO_2$  in ppm), dissolved  $CH_4$  concentration ( $CH_4$ , in  $\text{nmol L}^{-1}$ ), and  $N_2O$  saturation level**  
 572 **( $\%N_2O$ , in  $\%$ ) in four urban ponds (Leybeek (Leyb), Pêcheries (Pech), Tenreuken (Trk), and Silex (Slx)) in the city of Brussels**  
 573 **(Belgium) from June 2021 to December 2023. Box plots show median (horizontal line), mean (cross), and 25–75% percentiles (box**  
 574 **limits). Whiskers extend from minimum to maximum values. Grey and white bands in the plots on the right correspond to the**  
 575 **autumn/winter and spring/summer periods, respectively, and dotted vertical bars indicate the first day of each season. Lower case**  
 576 **letters indicate significant differences between ponds (Tables S3 and S4).**



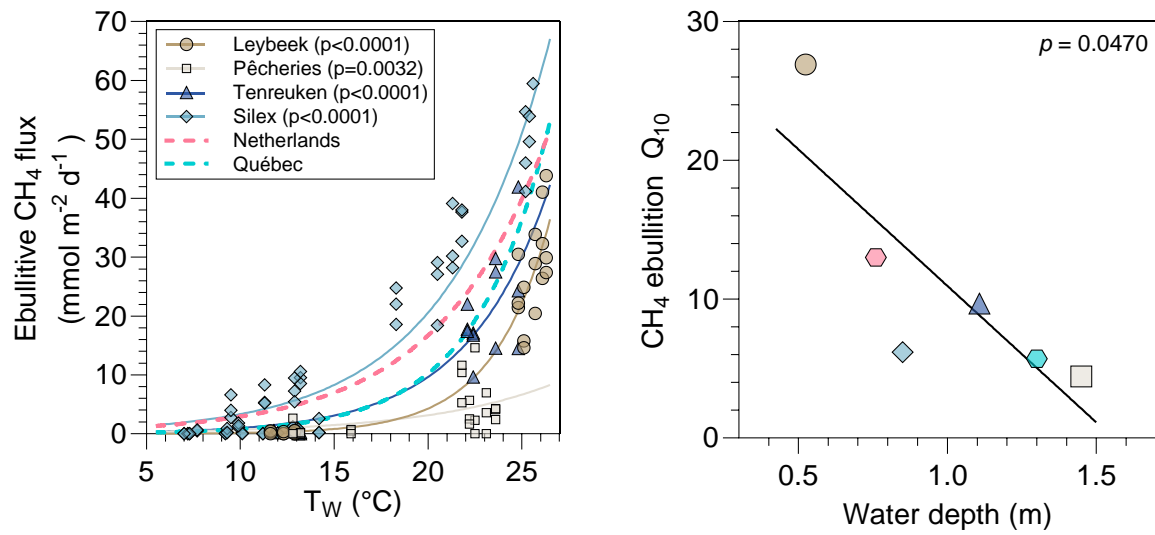
577

578 **Figure 4: Bubble flux ( $F_{\text{bubble}}$  in  $\text{mL m}^{-2} \text{d}^{-1}$ ) and the relative  $\text{CH}_4$  content in bubbles ( $\%\text{CH}_4$ , in %) as a function of surface water**  
579 **temperature ( $T_w$  in  $^{\circ}\text{C}$ ) in four urban ponds (Leybeek, Pêcherries, Tenreuken, and Silex) in the city of Brussels (Belgium) from**  
580 **June 2021 to December 2023. Bubbles fluxes were measured with three bubble traps in spring, summer, and fall of 2022 and 2023,**  
581 **totalling 8 days in the Leybeek, Pêcherries, and Tenreuken ponds and 24 days in the Silex pond. Given the shallowness of the**  
582 **sampled systems ( $<1.5$  m, Fig. 1), we assumed that sediments experience the same temperature as surface waters. In the upper**  
583 **plot, solid lines represent linear regression of  $\log_{10}(F_{\text{bubble}})$  as a function of  $T_w$  for the Leybeek ( $\log_{10}(F_{\text{bubble}}) = 0.0664 \times T_w +$**   
584  **$1.3095$ ,  $n=22$ ), the Pêcherries ( $\log_{10}(F_{\text{bubble}}) = 0.0486 \times T_w + 1.3257$ ,  $n=22$ ), the Tenreuken ( $\log_{10}(F_{\text{bubble}}) = 0.0492 \times T_w + 1.7039$ ,**  
585  **$n=19$ ), and the Silex ( $\log_{10}(F_{\text{bubble}}) = 0.0945 \times T_w + 1.0373$ ,  $n=72$ ) ponds. In the lower plot, solid line represents the linear regression**  
586 **of  $\%\text{CH}_4$  as a function of  $\log_{10}(T_w)$  for the Silex pond ( $\%\text{CH}_4 = 101.11 \times \log_{10}(T_w) - 87.8$ ,  $n=72$ ).**



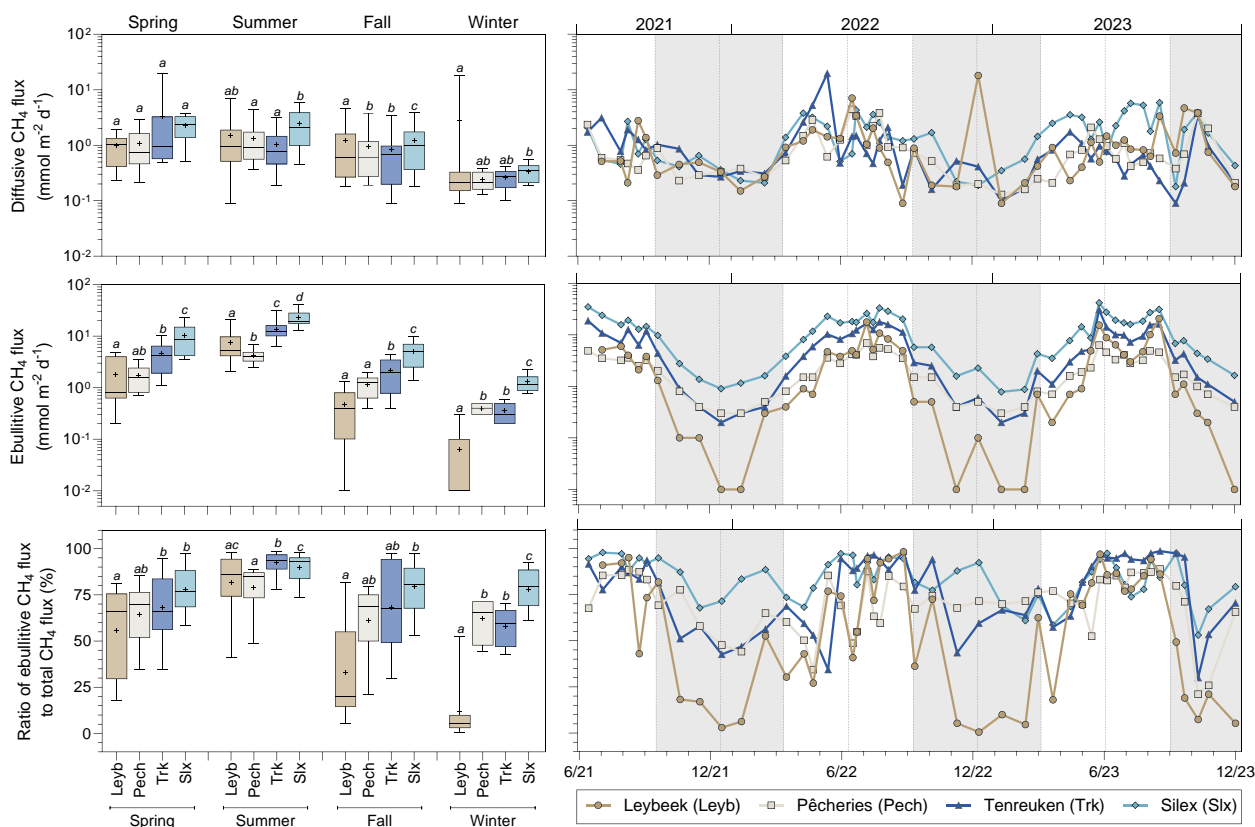
587

588 **Figure 5: Time-series of surface water temperature ( $T_w$ , °C), wind speed ( $\text{m s}^{-1}$ ), atmospheric pressure (atm), measured and**  
 589 **modeled bubble flux ( $F_{\text{bubble}}$  in  $\text{mL m}^{-2} \text{d}^{-1}$ ) in the Silex pond from the 29 March 2022 to the 15 April 2022 and from the 18 July 2022**  
 590 **to the 23 July 2022. The bubble flux was modelled from a fit to data based on  $T_w$  alone ( $\log_{10}(F_{\text{bubble}}) = 3.973 \times \log_{10}(T_w) -$**   
 591  **$2.15$ ,  $p < 0.0001$ ,  $n = 72$ ) and based on both  $T_w$  and drops in atmospheric pressure ( $\Delta p$ ) ( $\log_{10}(F_{\text{bubble}}) = 4.551 \times \log_{10}(T_w) +$**   
 592  **$1.962 \times \Delta p - 3.006$ ,  $p < 0.0001$ ,  $n = 72$ ).**



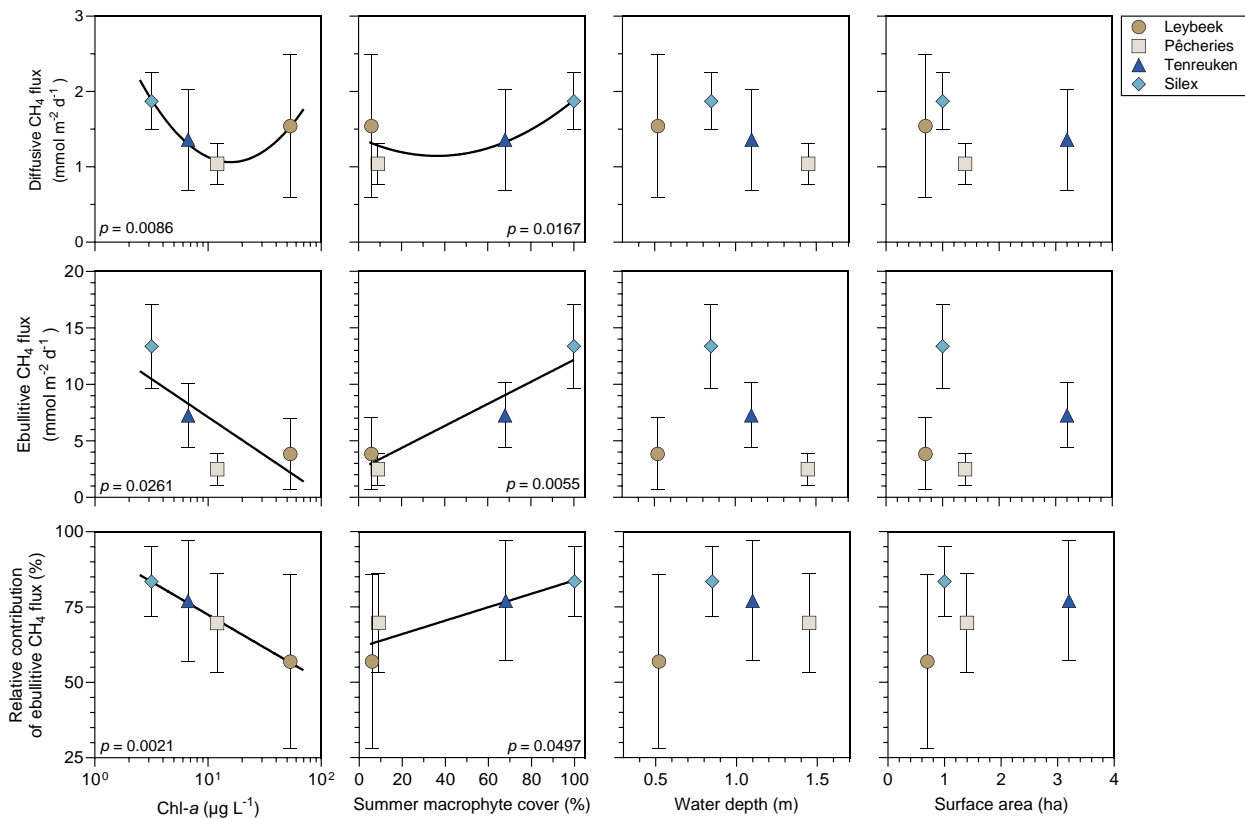
593

594 **Figure 6: Measured ebullitive CH<sub>4</sub> fluxes (mmol m<sup>-2</sup> d<sup>-1</sup>) as function of surface water temperature (°C) in four urban ponds**  
595 **(Leybeek, Pêcherries, Tenreuken, and Silex) in the city of Brussels (Belgium), in spring, summer, and fall of 2022 and 2023,**  
596 **totalling 8 days in the Leybeek, Pêcherries, and Tenreuken ponds and 24 days in the Silex pond, with three bubble traps. Solid lines**  
597 **represent exponential fit for the Leybeek ( $Y = 0.01 \cdot e^{0.32 \cdot X}$ ,  $n=22$ ), Pêcherries ( $Y = 0.16 \cdot e^{0.15 \cdot X}$ ,  $n=22$ ), Tenreuken ( $Y =$**   
598  **$0.10 \cdot e^{0.23 \cdot X}$ ,  $n=19$ ), Silex ( $Y = 0.54 \cdot e^{0.18 \cdot X}$ ,  $n=72$ ) ponds (Table S7). Dashed lines represent published exponential fit**  
599 **established in similar systems: four small ponds in Québec ( $Y = 0.06 \cdot e^{0.25 \cdot X}$ ) (DelSontro et al., 2016) and a small urban pond in**  
600 **the Netherlands ( $Y = 0.51 \cdot e^{0.17 \cdot X}$ ) (Aben et al., 2017). Each exponential curve allows to determine a Q<sub>10</sub> of CH<sub>4</sub> ebullition,**  
601 **plotted against water depth; solid line represents linear regression ( $Y = 30.64 - 19.67 \cdot X$ ,  $n = 6$ ).**



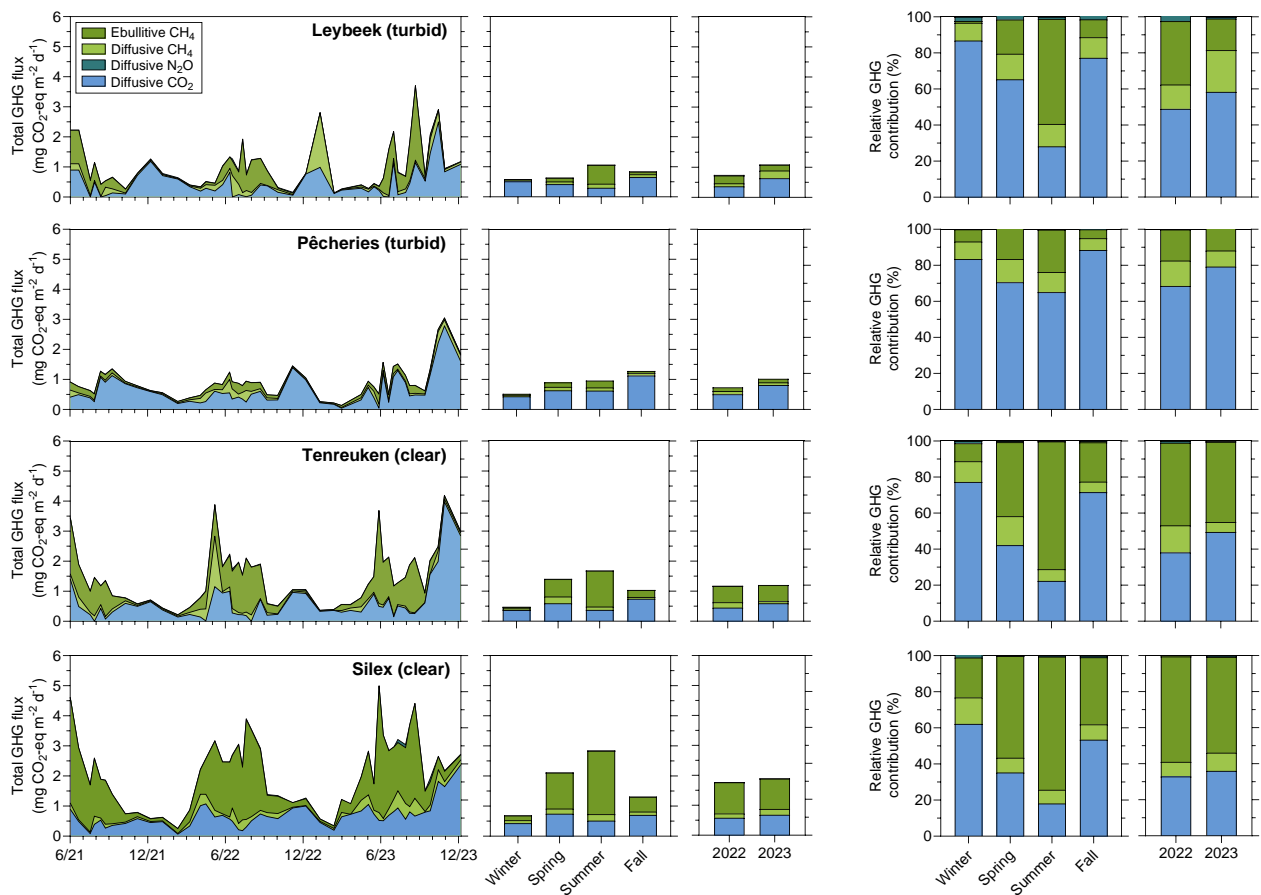
602

603 **Figure 7: Seasonal variations of diffusive and ebullitive CH<sub>4</sub> fluxes (mmol m<sup>-2</sup> d<sup>-1</sup>), and the ratio of ebullitive CH<sub>4</sub> flux to total**  
604 **(ebullitive+diffusive) CH<sub>4</sub> flux (%) in four urban ponds (Leybeek (Leyb), Pêcherries (Pech), Tenreuken (Trk), and Silex (Slx)) in the**  
605 **city of Brussels (Belgium) from June 2021 to December 2023. Diffusive fluxes were calculated from CH<sub>4</sub> concentration and gas**  
606 **transfer velocity derived from wind speed. Ebullitive CH<sub>4</sub> fluxes were calculated from the relations with water temperature for**  
607 **each pond (Fig. 6; Table S7) from the water temperature data coincident with the diffusive CH<sub>4</sub> fluxes. Note that the relations of**  
608 **ebullitive CH<sub>4</sub> fluxes as a function of water temperature were established over a temperature range (7.0 to 26.3°C) that is**  
609 **consistent with the range of water temperature values (2.0-25.9°C) over which the ebullitive CH<sub>4</sub> fluxes were modelled. Box plots**  
610 **show median (horizontal line), mean (cross), and 25–75% percentiles (box limits). Whiskers extend from minimum to maximum**  
611 **values. Grey and white bands in the plots on the right correspond to the autumn/winter and spring/summer periods, respectively,**  
612 **and dotted vertical bars indicate the first day of each season. Lower case letters indicate significant differences between ponds**  
613 **(Tables S3 and S4).**



614

615 **Figure 8: Mean diffusive and ebullitive CH<sub>4</sub> fluxes (mmol m<sup>-2</sup> d<sup>-1</sup>) and mean ratio of ebullitive CH<sub>4</sub> flux to total**  
616 **(diffusive+ebullitive) CH<sub>4</sub> flux (%) versus chlorophyll-*a* (Chl-*a*, in μg L<sup>-1</sup>), total macrophyte cover in summer (%), water depth**  
617 **(m), and lake surface area (ha) in four ponds (Leybeek, Pêcherries, Tenreuken, and Silex) in the city of Brussels (Belgium) from**  
618 **June 2021 to December 2023. Error bars indicate the standard deviation. Solid lines indicate either linear or polynomial fits.**  
619 **Statistical comparisons between the four ponds are summarized in Table S3.**



620

621 **Figure 9: Seasonal and year-to-year variations of the emissions to the atmosphere of CO<sub>2</sub> (diffusive), CH<sub>4</sub> (diffusive and ebullitive),**  
 622 **and N<sub>2</sub>O (diffusive) expressed in CO<sub>2</sub> equivalents (in mg CO<sub>2</sub>-eq m<sup>-2</sup> d<sup>-1</sup>) and their relative contribution in %, in four urban ponds**  
 623 **(Leybeek, Pêcherries, Tenreuken, and Silex) in the city of Brussels (Belgium) from June 2021 to December 2023. Seasonal averages**  
 624 **include data from 2021, 2022, and 2023. The annual precipitation was higher in 2023 (1011 mm) than in 2022 (701 mm).**

625 **Data availability.** The full data-set is available at 10.5281/zenodo.11103556.

626 **Author contributions.** AVB and NG conceived the study; TB collected field samples; TB and AVB made the laboratory  
627 analysis; TB and AVB jointly interpreted data and drafted the manuscript with substantial inputs from NG.

628 **Competing interests.** The authors declare that they have no conflict of interest.

629 **Acknowledgements.** We thank Ozan Efe (University of Liège) and Adriana Anzil (Université Libre de Bruxelles) for  
630 analytical assistance, Florence Charlier (Université Libre de Bruxelles) for help in macrophyte identification and density  
631 quantification (Table S1), Bruxelles Environnement for providing information on history of operations in the ponds (Table  
632 S2), two anonymous reviewers and Associate Editor (Gabriel Singer) for comments and suggestions on the initial  
633 manuscript.

634 **Financial support.** TB received funding from the Brussels-Capital Region’s institute for the encouragement of scientific  
635 research and innovation (Innoviris) as part of the Smartwater project (RBC/2020-EPF-6 h) and from the “Fonds pour la  
636 formation à la Recherche dans l’Industrie et dans l’Agriculture” (FRIA, Belgium). AVB is a Research Director at the FRS-  
637 FNRS.

## 638 **References**

- 639 Aben, R. C. H., Barros, N., Van Donk, E., Frenken, T., Hilt, S., Kazanjian, G., Lamers, L. P. M., Peeters, E. T. H. M.,  
640 Roelofs, J.G.M., de Senerpont Domis, L. S., Stephan, S., Velthuis, M., Van de Waal, D., Wik, M., Thornton, B.,  
641 Wilkinson, J., Delsontro, T., and Kosten, S.: Cross continental increase in methane ebullition under climate change.  
642 *Nature communications*, 8(1), 1682. <https://doi.org/10.1038/s41467-017-01535-y>, 2017.
- 643 Audet, J., Neif, É.M., Cao, Y., Hoffmann, C.C., Lauridsen, T.L., Larsen, S.E., Søndergaard, M., Jeppesen, E., and Davidson,  
644 T.A.: Heat-wave effects on greenhouse gas emissions from shallow lake mesocosms. *Freshwater*  
645 *Biology*. 2017; 62: 1130–1142. <https://doi.org/10.1111/fwb.12930>, 2017.
- 646 Audet, J., Carstensen, M.V., Hoffmann, C.C., Lavaux, L., Thiemer, K., and Davidson, T.A.: Greenhouse gas emissions from  
647 urban ponds in Denmark. *Inland Waters*, 10 (3), 373–385. <https://doi.org/10.1080/20442041.2020.1730680>, 2020.
- 648 Baliña, S., Sanchez, M. L., Izaguirre, I., and del Giorgio, P. A.: Shallow lakes under alternative states differ in the dominant  
649 greenhouse gas emission pathways. *Limnology and Oceanography*, 68(1), 1-13. <https://doi.org/10.1002/lno.12243>,  
650 2023.
- 651 Barko, J. W., Gunnison, D., and Carpenter, S. R.: Sediment interactions with submersed macrophyte growth and community  
652 dynamics. *Aquatic botany*, 41(1-3), 41-65. [https://doi.org/10.1016/0304-3770\(91\)90038-7](https://doi.org/10.1016/0304-3770(91)90038-7), 1991.
- 653 Bartosiewicz, M., Maranger, R., Przytulska, A., and Laurion, I.: Effects of phytoplankton blooms on fluxes and emissions of  
654 greenhouse gases in a eutrophic lake. *Water Research*, 196, 116985. <https://doi.org/10.1016/j.watres.2021.116985>,  
655 2021.
- 656 Bastviken, D., Ejlertsson, J. and Tranvik, L.: Measurement of methane oxidation in lakes: A comparison of methods.  
657 *Environmental Science & Technology*, 36, 3354-3361. <https://doi.org/10.1021/es010311p>, 2002.
- 658 Bastviken, D., Treat, C.C., Pangala, S.R., Gauci, V., Enrich-Prast, A., Karlson, M., Gålfalk, M., Romano, M.B., and  
659 Sawakuchi, H.O.: The importance of plants for methane emission at the ecosystem scale. *Aquatic Botany*, 184,  
660 103596. <https://doi.org/10.1016/j.aquabot.2022.103596>, 2023.
- 661 Bates, D., Maechler, M., Bolker, B., and Walker, S.: Fitting linear mixed-effects models using lme4. *Journal of Statistical*  
662 *Software*, 67, 1–48. <https://doi.org/10.1126/science.1176170>, 2015.

663 Bauduin, T., Gypens, N., and Borges, A.V.: Seasonal and spatial variations of greenhouse gas (CO<sub>2</sub>, CH<sub>4</sub> and N<sub>2</sub>O)  
664 emissions from urban ponds in Brussels. *Water Research*, 121257. <https://doi.org/10.1016/j.watres.2024.121257>,  
665 2024.

666 Borges, A.V., Darchambeau, F., Lambert, T., Morana, C., Allen, G.H., Tambwe, E., and Bouillon, S.: Variations in  
667 dissolved greenhouse gases (CO<sub>2</sub>, CH<sub>4</sub>, N<sub>2</sub>O) in the Congo River network overwhelmingly driven by fluvial-  
668 wetland connectivity. *Biogeosciences*, 16 (19), 3801–3834. <https://doi.org/10.5194/bg-16-3801-2019>, 2019.

669 Borges, A.V., Deirmendjian, L., Bouillon, S., Okello, W., Lambert, T., Roland, F.A.E., Razanamahandry, V.F., Voarintsoa,  
670 N.R.G., Darchambeau, F., Kimirei, I.A., Descy, J., Allen, G.H., and Morana, C.: Greenhouse gas emissions from  
671 African lakes are no longer a blind spot. *Sciences Advances*, 8 (25), eabi8716. <https://doi.org/10.1126/sciadv.abi8716>, 2022.

673 Borges, A.V., Okello, W., Bouillon, S., Deirmendjian, S., Nankabirwa, A., Nabafu, E., Lambert, T., Descy, J-P, and Morana,  
674 C.: Spatial and temporal variations of dissolved CO<sub>2</sub>, CH<sub>4</sub> and N<sub>2</sub>O in Lakes Edward and George (East Africa).  
675 *Journal of Great Lakes Research*, 49, 229-245, <https://doi.org/10.1016/j.jglr.2022.11.010>, 2023.

676 Brans, K.I., Engelen, J.M., Souffreau, C., and De Meester, L.: Urban hot-tubs: local urbanization has profound effects on  
677 average and extreme temperatures in ponds. *Landscape and Urban Planning*, 176, 22–29. <https://doi.org/10.1016/j.landscapeurbplan.2018.04.019>,  
678 2018.

679 Cael, B. B., Heathcote, A. J., and Seekell, D. A.: The volume and mean depth of Earth's lakes. *Geophysical Research*  
680 *Letters*, 44(1), 209-218. <https://doi.org/10.1002/2016GL071378>, 2017.

681 Casas-Ruiz, J.P., Jakobsson, J., and del Giorgio, P.A.: The role of lake morphometry in modulating surface water carbon  
682 concentrations in boreal lakes. *Environmental Research Letters*, 16 (7), 074037 <https://doi.org/10.1088/1748-9326/ac0be3>, 2021.

684 Chen, B., Zhang, L., and Wang, C.: Distinct impacts of the central and eastern Atlantic Niño on the European climate.  
685 *Geophysical Research Letters*, 51(2), e2023GL107012. <https://doi.org/10.1029/2023GL107012>, 2024.

686 Choudhury, M. I., McKie, B. G., Hallin, S., and Ecke, F.: Mixtures of macrophyte growth forms promote nitrogen cycling in  
687 wetlands. *Science of the Total Environment*, 635, 1436-1443. <https://doi.org/10.1016/j.scitotenv.2018.04.193>, 2018.

688 Clifford, C.C., and Heffernan, J.B.: Artificial aquatic ecosystems. *Water*, 10 (8), 1096. <https://doi.org/10.3390/w10081096>,  
689 2018.

690 Codispoti, L.A., and Christensen, J.P.: Nitrification, denitrification and nitrous oxide cycling in the eastern tropical South  
691 Pacific Ocean. *Marine chemistry*, 16 (4), 277–300. [https://doi.org/10.1016/0304-4203\(85\)90051-9](https://doi.org/10.1016/0304-4203(85)90051-9), 1985.

692 Cole, J.J., and Caraco, N.F.: Atmospheric exchange of carbon dioxide in a low-wind oligotrophic lake measured by the  
693 addition of SF<sub>6</sub>. *Limnology and Oceanography*, 43 (4), 647–656. <https://doi.org/10.4319/lo.1998.43.4.0647>, 1998.

694 Dan, Z., Chuan, W., Qiaohong, Z., and Xingzhong, Y.: Sediments nitrogen cycling influenced by submerged macrophytes  
695 growing in winter. *Water Science and Technology*, 83(7), 1728-1738. <https://doi.org/10.2166/wst.2021.081>, 2021.

696 Davidson, T.A., Audet, J., Svenning, J.C., Lauridsen, T.L., Søndergaard, M., Landkildehus, F., and Jeppesen, E.:  
697 Eutrophication effects on greenhouse gas fluxes from shallow-lake mesocosms override those of climate warming.  
698 *Global Change Biology*, 21 (12), 4449–4463. <https://doi.org/10.1111/gcb.13062>, 2015.

699 Deemer, B. R., and Holgerson, M. A.: Drivers of methane flux differ between lakes and reservoirs, complicating global  
700 upscaling efforts. *Journal of Geophysical Research: Biogeosciences*, 126(4) <https://doi.org/10.1029/2019JG005600>  
701 , 2021.

702 DelSontro, T., Beaulieu, J. J., and Downing, J. A.: Greenhouse gas emissions from lakes and impoundments: Upscaling in  
703 the face of global change. *Limnology and Oceanography Letters*, 3(3), 64-75. <https://doi.org/10.1002/lo2.10073>,  
704 2018.

705 DelSontro, T., Kunz, M. J., Kempster, T., Wüest, A., Wehrli, B., and Senn, D. B.: Spatial Heterogeneity of Methane  
706 Ebullition in a Large Tropical Reservoir, *Environmental Science & Technology*, 45 (23), 9866-9873,  
707 <https://doi.org/10.1021/es2005545>, 2011.

708 DelSontro, T., Boutet, L., St-Pierre, A., del Giorgio, P.A., and Prairie, Y.T.: Methane ebullition and diffusion from northern  
709 ponds and lakes regulated by the interaction between temperature and system productivity, *Limnology and*  
710 *Oceanography*, 61(S1), S62-S77 <https://doi.org/10.1002/lno.10335>, 2016.

711 Deng, Hg., Zhang, J., Wu, J., Yao, X., and Yang, L.-W.: Biological denitrification in a macrophytic lake: implications for  
712 macrophytes-dominated lake management in the north of China. *Environmental Sciences and Pollution Research*,  
713 27, 42460–42471. <https://doi.org/10.1007/s11356-020-10230-3>, 2020.

714 Desrosiers, K., DelSontro, T., and del Giorgio, P.A.: Disproportionate Contribution of Vegetated Habitats to the CH<sub>4</sub> and  
715 CO<sub>2</sub> Budgets of a Boreal Lake. *Ecosystems*, 1-20. <https://doi.org/10.1007/s10021-021-00730-9>, 2022.

716 Dickson, A.G.; Sabine, C.L. and Christian, J.R.: Guide to best practices for ocean CO<sub>2</sub> measurement. Sidney, British  
717 Columbia, North Pacific Marine Science Organization, 191pp. (PICES Special Publication 3; IOCCP Report 8).  
718 <https://doi.org/10.25607/OBP-1342>, 2007.

719 Dutton, G., Elkins II, J., Hall, B., NOAA ESRL, Earth System Research Laboratory Halocarbons and Other Atmospheric  
720 Trace Gases Chromatograph for Atmospheric Trace Species (CATS) Measurements. NOAA National Centers for  
721 Environmental Information. <https://doi.org/10.7289/V5X0659V>. Version 1. [Database: atmospheric nitrous oxide  
722 N<sub>2</sub>O] [2024-03-27], 2023.

723 Goeckner, A. H., Lusk, M. G., Reisinger, A. J., Hosen, J. D., and Smoak, J. M.: Florida's urban stormwater ponds are net  
724 sources of carbon to the atmosphere despite increased carbon burial over time. *Communications earth &*  
725 *environment*, 3(1), 53, <https://doi.org/10.1038/s43247-022-00384-y> 2022.

726 Gorsky, A. L., Dugan, H. A., Wilkinson, G. M., and Stanley, E. H.: Under-ice oxygen depletion and greenhouse gas  
727 supersaturation in north temperate urban ponds. *Journal of Geophysical Research: Biogeosciences*, 129(6),  
728 <https://doi.org/10.1029/2024JG008120>, 2024.

729 Gorsky, A.L., Racanelli, G.A., Belvin, A.C., and Chambers, R.M.: Greenhouse gas flux from stormwater ponds in  
730 southeastern Virginia (USA). *Anthropocene*, 28, 100218. <https://doi.org/10.1016/j.ancene.2019.100218>, 2019.

731 Grasset, C., Abril, G., Mendonça, R., Roland, F., and Sobek, S.: The transformation of macrophyte-derived organic matter to  
732 methane relates to plant water and nutrient contents. *Limnology and Oceanography*, 64(4), 1737-1749,  
733 <https://doi.org/10.1002/lno.11148>, 2019.

734 Grasset, C., Sobek, S., Scharnweber, K., Moras, S., Villwock, H., Andersson, S., Hiller, C., Nydahl, A.C., Chaguaceda, F.,  
735 Colom, W., and Tranvik, L.J.: The CO<sub>2</sub>-equivalent balance of freshwater ecosystems is non-linearly related to  
736 productivity. *Global Change Biology*, 26 (10), 5705–5715. <https://doi.org/10.1111/gcb.15284>, 2020.

737 Grasshoff, K., and Johannsen, H.: A new sensitive and direct method for the automatic determination of ammonia in sea  
738 water. *ICES Journal of Marine Science*, 34 (3), 516–521. <https://doi.org/10.1093/icesjms/34.3.516>, 1972.

739 Grasshoff, K., Kremling, K., and Ehrhardt, M.: Methods of Seawater Analysis: Determination of Nitrite. John Wiley & Sons,  
740 2009.

741 Grinham, A., Albert, S., Deering, N., Dunbabin, M., Bastviken, D., Sherman, B., Lovelock, C.E., and Evans, C.D.: The  
742 importance of small artificial water bodies as sources of methane emissions in Queensland, Australia. *Hydrology*  
743 *and Earth System Sciences*, 22 (10), 5281–5298. <https://doi.org/10.5194/hess-22-5281-2018>, 2018.

744 Harpenslager, S. F., Thiemer, K., Levertz, C., Misteli, B., Sebola, K. M., Schneider, S. C., Hilt, S., and Köhler, J.: Short-term  
745 effects of macrophyte removal on emission of CO<sub>2</sub> and CH<sub>4</sub> in shallow lakes. *Aquatic Botany*, 182, 103555.  
746 <https://doi.org/10.1016/j.aquabot.2022.103555>, 2022.

747 Hassall, C., The ecology and biodiversity of urban ponds. *WIREs Water*, 1: 187-206. <https://doi.org/10.1002/wat2.1014>,  
748 2014.

749 Herrero Ortega, S., Romero Gonz´alez-Quijano, C., Casper, P., Singer, G.A., and Gessner, M.O.: Methane emissions from  
750 contrasting urban freshwaters: rates, drivers, and a whole-city footprint. *Global change biology*, 25 (12), 4234–  
751 4243. <https://doi.org/10.1111/gcb.14799>, 2019.

- 752 Hilt, S., Brothers, S., Jeppesen, E., Veraart, A. J., and Kosten, S.: Translating regime shifts in shallow lakes into changes in  
753 ecosystem functions and services. *BioScience*, 67(10), 928-936. <https://doi.org/10.1093/biosci/bix106>, 2017.
- 754 Holgerson, M., and Raymond, P.: Large contribution to inland water CO<sub>2</sub> and CH<sub>4</sub> emissions from very small ponds. *Nature*  
755 *Geoscience*, 9, 222–226. <https://doi.org/10.1038/ngeo2654>, 2016.
- 756 Holgerson, MA.: Drivers of carbon dioxide and methane supersaturation in small, temporary ponds, *Biogeochemistry*, 124,  
757 305–318. <https://doi.org/10.1007/s10533-015-0099-y>, 2015.
- 758 Huttunen, J. T., Alm, J., Liikanen, A., Juutinen, S., Larmola, T., Hammar, T., Silvola, T., and Martikainen, P. J.: Fluxes of  
759 methane, carbon dioxide and nitrous oxide in boreal lakes and potential anthropogenic effects on the aquatic  
760 greenhouse gas emissions. *Chemosphere*, 52(3), 609-621. [https://doi.org/10.1016/S0045-6535\(03\)00243-1](https://doi.org/10.1016/S0045-6535(03)00243-1), 2003.
- 761 Hyvönen, T., Ojala, A., Kankaala, P., & Martikainen, P. J.: Methane release from stands of water horsetail (*Equisetum*  
762 *fluviatile*) in a boreal lake, *Freshwater Biology*, 40, 275– 284. <https://doi.org/10.1046/j.1365-2427.1998.00351.x>,  
763 1998.
- 764 Johnson, M.S., Matthews, E., Du, J., Genovese, V., and Bastviken, D.: Methane Emission from Global Lakes: New  
765 Spatiotemporal Data and Observation-Driven Modeling of Methane Dynamics Indicates Lower Emissions. *Journal*  
766 *of Geophysical Research: Biogeosciences*, 127(7). <https://doi.org/10.1029/2022JG006793>, 2022.
- 767 Juutinen, S., Alm, J., Larmola, T., Huttunen, J. T., Morero, M., Martikainen, P. J., and Silvola, J.: Major implication of the  
768 littoral zone for methane release from boreal lakes, *Global biogeochemical cycles*, 17(4), 1117,  
769 <https://doi.org/10.1029/2003GB002105>, 2003.
- 770 Kankaala, P., Huotari, J., Tulonen, T., and Ojala, A.: A Lake-size dependent physical forcing drives carbon dioxide and  
771 methane effluxes from lakes in a boreal landscape. *Limnology and Oceanography*, 58:1915–1930.  
772 <https://doi.org/10.4319/lo.2013.58.6.1915>, 2013.
- 773 Keller, M., and Stallard, R. F.: Methane emission by bubbling from Gatun Lake, Panama, *Journal of Geophysical Research:*  
774 *Atmospheres*, 99(D4), 8307–8319, doi:10.1029/92JD02170, 1994.
- 775 Koroleff, J.: Determination of total phosphorus by alkaline persulphate oxidation. *Methods of Seawater Analysis*. Verlag  
776 Chemie, Wienheim, pp. 136–138, 1983.
- 777 Kosten, S., Roland, F., Da Motta Marques, D. M., Van Nes, E. H., Mazzeo, N., Sternberg, L. D. S., Scheffer, M., and Cole,  
778 J. J. Climate-dependent CO<sub>2</sub> emissions from lakes. *Global Biogeochemical Cycles*, 24(2).  
779 <https://doi.org/10.1029/2009GB003618>, 2010.
- 780 Lan, X., K.W. Thoning, and E.J. Dlugokencky: Trends in globally-averaged CH<sub>4</sub>, N<sub>2</sub>O, and SF<sub>6</sub> determined from NOAA  
781 Global Monitoring Laboratory measurements [data set]. Version 2024-08, <https://doi.org/10.15138/P8XG-AA10>,  
782 2024.
- 783 Lauerwald, R., Regnier, P., Figueiredo, V., Enrich-Prast, A., Bastviken, D., Lehner, B., Maavara, T., and Raymond, P.:  
784 Natural Lakes Are a Minor Global Source of N<sub>2</sub>O to the Atmosphere. *Global Biogeochemical Cycles*, 33(12),  
785 1564–1581. <https://doi.org/10.1029/2019GB006261>, 2019.
- 786 Lauerwald, R., Allen, G. H., Deemer, B. R., Liu, S., Maavara, T., Raymond, P., Alcott, L., Bastviken, D., Hastie, A.,  
787 Holgerson, M.A., Johnson, M. S., Lehner, B., Lin, P., Marzadri, A., Ran, L., Tian, H., Yang, X., Yao, Y., and  
788 Regnier, P.: Inland water greenhouse gas budgets for RECCAP2: 2. Regionalization and homogenization of  
789 estimates. *Global Biogeochemical Cycles*, 37, e2022GB007658. <https://doi.org/10.1029/2022GB007658>, 2023.
- 790 Liu, W., Jiang, X., Zhang, Q., Li, F., and Liu, G.: Has submerged vegetation loss altered sediment denitrification, N<sub>2</sub>O  
791 production, and denitrifying microbial communities in subtropical lakes? *Global Biogeochemical Cycles*, 32, 1195–  
792 1207. <https://doi.org/10.1029/2018GB005978>, 2018.
- 793 Maavara, T., Lauerwald, R., Laruelle, G. G., Akbarzadeh, Z., Bouskill, N. J., Van Cappellen, P., and Regnier, P.: Nitrous  
794 oxide emissions from inland waters: Are IPCC estimates too high? *Global Change Biology*, 25(2), 473–488.  
795 <https://doi.org/10.1111/gcb.145042>, 2019.

796 Marotta, H., Duarte, C. M., Pinho, L., and Enrich-Prast, A.: Rainfall leads to increased pCO<sub>2</sub> in Brazilian coastal lakes.  
797 *Biogeosciences*, 7(5), 1607–1614. <https://doi.org/10.5194/bg-7-1607-2010>, 2010.

798 Martinez-Cruz, K., Gonzalez-Valencia, R., Sepulveda-Jauregui, A., Plascencia- Hernandez, F., Belmonte-Izquierdo, Y., and  
799 Thalasso, F.: Methane emission from aquatic ecosystems of Mexico City. *Aquatic Sciences*, 79, 159–169.  
800 <https://doi.org/10.1007/s00027-016-0487-y>, 2017.

801 Mengis, M., Gächter, R., and Wehrli, B.: Sources and sinks of nitrous oxide (N<sub>2</sub>O) in deep lakes. *Biogeochemistry*, 38, 281–  
802 301. <https://doi.org/10.1023/A:1005814020322>, 1997.

803 Myrhe, G., Shindell, D., Bréon, F.M., Collins, W., and Al, E. Anthropogenic and natural radiative forcing. Climate Change  
804 2013 the Physical Science Basis: working Group I Contribution to the Fifth Assessment Report of the  
805 Intergovernmental Panel on Climate Change. Chapter 8 : Anthropogenic and Natural Radiative Forcing  
806 9781107057, 659–740. <https://doi.org/10.1017/CBO9781107415324.018>, 2013.

807 Natchimuthu, S., Panneer Selvam, B., and Bastviken, D.: Influence of weather variables on methane and carbon dioxide flux  
808 from a shallow pond. *Biogeochemistry*, 119, 403–413. <https://doi.org/10.1007/s10533-014-9976-z>, 2014.

809 Natchimuthu, S., Sundgren, I., Gålfalk, M., Klemetsson, L., Crill, P., Danielsson, Å. and Bastviken, D. (2016), Spatio-  
810 temporal variability of lake CH<sub>4</sub> fluxes and its influence on annual whole lake emission estimates. *Limnology and*  
811 *Oceanography*, 61: S13-S26. <https://doi.org/10.1002/lno.10222>, 2016.

812 Ni, M., Liang, X., Hou, L., Li, W., and He, C.: Submerged macrophytes regulate diurnal nitrous oxide emissions from a  
813 shallow eutrophic lake: A case study of Lake Wuliangsu in the temperate arid region of China. *Science of The*  
814 *Total Environment*, 811, 152451. <https://doi.org/10.1016/j.scitotenv.2021.152451>, 2022.

815 Ojala A., Bellido J.L., Tulonen T., Kankaala P., and Huotari J.: Carbon gas fluxes from a brown-water and a clear-water lake  
816 in the boreal zone during a summer with extreme rain events, *Limnology and Oceanography*, 56,  
817 <https://doi.org/10.4319/lo.2011.56.1.0061>, 2011.

818 Ollivier, Q.R., Maher, D.T., Pitfield, C., and Macreadie, P.I.: Punching above their weight: large release of greenhouse gases  
819 from small agricultural dams. *Global change biology*, 25 (2), 721–732. <https://doi.org/10.1111/gcb.14477>, 2019.

820 Peacock, M., Audet, J., Bastviken, D., Cook, S., Evans, C.D., Grinham, A., Holgerson, M. A., Högbom, L., Pickard, A.E.,  
821 Zieliński, P., and Fitter, M.N.: Small artificial waterbodies are widespread and persistent emitters of methane and  
822 carbon dioxide. *Global change biology*, 27 (20), 5109–5123. <https://doi.org/10.1111/gcb.15762>, 2021.

823 Peacock, M., Audet, J., Jordan, S., Smeds, J., and Wallin, M.B.: Greenhouse gas emissions from urban ponds are driven by  
824 nutrient status and hydrology. *Ecosphere*, 10 (3), e02643. <https://doi.org/10.1002/ecs2.2643>, 2019.

825 Peretyatko, A., Symoens, J. J., and Triest, L.: Impact of macrophytes on phytoplankton in eutrophic peri-urban ponds,  
826 implications for pond management and restoration. *Belgian Journal of Botany*, 83-99.  
827 <https://doi.org/10.2307/20794626>, 2007.

828 R Core Team (2021). R: A language and environment for statistical computing. R Foundation for Statistical Computing,  
829 Vienna, Austria. <https://www.R-project.org/>, 2021.

830 Rabaey, J. and Cotner, J.: Pond greenhouse gas emissions controlled by duckweed coverage. *Frontiers in environmental*  
831 *science*, 10, 889289 <https://doi.org/10.3389/fenvs.2022.889289>, 2022.

832 Rabaey, J. and Cotner, J.: The influence of mixing on seasonal carbon dioxide and methane fluxes in ponds.  
833 *Biogeochemistry*, 1-18, <https://doi.org/10.1007/s10533-024-01167-7>, 2024.

834 Rasilo, T., Ojala, A., Huotari, J. and Pumpanen, J.: Rain Induced Changes in Carbon Dioxide Concentrations in the Soil–  
835 Lake–Brook Continuum of a Boreal Forested Catchment. *Vadose Zone Journal*, 11: vzj2011.0039.  
836 <https://doi.org/10.2136/vzj2011.0039>, 2012.

837 Ray, N. E., and Holgerson, M. A.: High Intra-Seasonal Variability in Greenhouse Gas Emissions from Temperate  
838 Constructed Ponds. *Geophysical Research Letters*, 50(18), e2023GL104235,  
839 <https://doi.org/10.1029/2023GL104235>, 2023.

840 Ray, N. E., Holgerson, M. A., Andersen, M. R., Bikše, J., Bortolotti, L. E., Futter, M., Kokorite, I., Law, A., McDonald, C.,  
841 Mesman, J.P., Peacock, M., Richardson, D.C., Arsenault, J., Bansal, S., Cawley, K., Kuhn, M., Shahabinia, A.R.,  
842 and Smufer, F.: Spatial and temporal variability in summertime dissolved carbon dioxide and methane in  
843 temperate ponds and shallow lakes. *Limnology and Oceanography*, 68(7), 1530-1545.  
844 <https://doi.org/10.1002/lno.12362>, 2023.

845 Raymond, P. A., Hartmann, J., Lauerwald, R., Sobek, S., McDonald, C., Hoover, M., Butman, D., Striegl, R., Mayorga, E.,  
846 Humborg, C., Kortelainen, P., Dürr, H., Meybeck, M., Ciais, P., and Guth, P.: Global carbon dioxide emissions  
847 from inland waters. *Nature*, 503(7476), 355–359. <https://doi.org/10.1038/nature12760>, 2013.

848 Reitsema, R. E., Meire, P., and Schoelynck, J.: The future of freshwater macrophytes in a changing world: dissolved organic  
849 carbon quantity and quality and its interactions with macrophytes. *Frontiers in Plant Science*, 9, 301954.  
850 <https://doi.org/10.3389/fpls.2018.00629>, 2018.

851 Rocher-Ros, G., Stanley, E. H., Loken, L. C., Casson, N. J., Raymond, P. A., Liu, S., Amatulli, G., and Sponseller, R. A.:  
852 Global methane emissions from rivers and streams. *Nature*, 621:530–535. [https://doi.org/10.1038/s41586-023-](https://doi.org/10.1038/s41586-023-06344-6)  
853 [06344-6](https://doi.org/10.1038/s41586-023-06344-6), 2023.

854 Rosentreter, J. A., Borges, A. V., Deemer, B. R., Holgerson, M. A., Liu, S., Song, C., Melack, J., Raymond, P. A., Duarte, C.  
855 M., Allen, G. H., Olefeldt, D., Poulter, B., Battin, T. I., and Eyre, B. D.: Half of global methane emissions come  
856 from highly variable aquatic ecosystem sources. *Nature Geoscience*, 14(4), 225–230.  
857 <https://doi.org/10.1038/s41561-021-00715-2>, 2021.

858 Sand-Jensen, K., & Staehr, P. A.: Scaling of pelagic metabolism to size, trophy and forest cover in small Danish lakes.  
859 *Ecosystems*, 10, 128-142. <https://doi.org/10.1007/s10021-006-9001-z>, 2007.

860 Scandella, B. P., Varadharajan, C., Hemond, H. F., Ruppel, C., and Juanes, R.: A conduit dilation model of methane venting  
861 from lake sediments. *Geophysical Research Letters*, 38(6). <https://doi.org/10.1029/2011GL046768>, 2011.

862 Scheffer, M., Hosper, S. H., Meijer, M. L., Moss, B., and Jeppesen, E.: Alternative equilibria in shallow lakes. *Trends in*  
863 *ecology & evolution*, 8(8), 275-279. [https://doi.org/10.1016/0169-5347\(93\)90254-M](https://doi.org/10.1016/0169-5347(93)90254-M), 1993.

864 Schulz, S. and Conrad, R.: Influence of temperature on pathways to methane production in the permanently cold profundal  
865 sediment of Lake Constance. *FEMS Microbiology Ecology*, 20 1-14; [https://doi.org/10.1111/j.1574-](https://doi.org/10.1111/j.1574-6941.1996.tb00299.x)  
866 [6941.1996.tb00299.x](https://doi.org/10.1111/j.1574-6941.1996.tb00299.x), 1996.

867 Singh, S.N., Kulshreshtha, K., and Agnihotri, S.: Seasonal dynamics of methane emission from wetlands. *Chemosphere-*  
868 *Global Change Science*, 2 (1), 39–46. [https://doi.org/10.1016/S1465-9972\(99\)00046-X](https://doi.org/10.1016/S1465-9972(99)00046-X), 2000.

869 Stanley, E. H., Casson, N. J., Christel, S. T., Crawford, J. T., Loken, L. C., and Oliver, S. K.: The ecology of methane in  
870 streams and rivers: patterns, controls, and global significance. *Ecological Monographs*, 86(2), 146–171.  
871 <https://doi.org/10.1890/15-1027>, 2016.

872 Taoka, T., Iwata, H., Hirata, R., Takahashi, Y., Miyabara, Y., and Itoh, M.: Environmental controls of diffusive and  
873 ebullitive methane emissions at a subdaily time scale in the littoral zone of a midlatitude shallow lake. *Journal of*  
874 *Geophysical Research: Biogeosciences*, 125, e2020JG005753. <https://doi.org/10.1029/2020JG005753>, 2020.

875 Theus, M. E., Ray, N. E., Bansal, S., and Holgerson, M. A.: Submersed macrophyte density regulates aquatic greenhouse gas  
876 emissions. *Journal of Geophysical Research: Biogeosciences*, 128(10), <https://doi.org/10.1029/2023JG007758>,  
877 2023.

878 Tixier, G., M Lafont, M., L Grapentine, L., Q Rochfort, Q., and J Marsalek, J.: Ecological risk assessment of urban  
879 stormwater ponds: Literature review and proposal of a new conceptual approach providing ecological quality goals  
880 and the associated bioassessment tools, *Ecological Indicators*, 11, 1497-1506,  
881 <https://doi.org/10.1016/j.ecolind.2011.03.027>, 2011.

882 Tokida, T., Miyazaki, T., Mizoguchi, M., Nagata, O., Takakai, F., Kagemoto, A., and Hatano, R.: Falling atmospheric  
883 pressure as a trigger for methane ebullition from peatland. *Global Biogeochemical Cycles*, 21(2).  
884 <https://doi.org/10.1029/2006GB002790>, 2007.

885 Vachon, D., and del Giorgio, P.A. Whole-Lake CO<sub>2</sub> Dynamics in Response to Storm Events in Two Morphologically  
886 Different Lakes. *Ecosystems*, 17, 1338–1353 (2014). <https://doi.org/10.1007/s10021-014-9799-8>, 2014.

887 Vachon, D., Langenegger, T., Donis, D., Beaubien, S. E., and McGinnis, D. F.: Methane emission offsets carbon dioxide  
888 uptake in a small productive lake. *Limnology and Oceanography Letters*, 5(6), 384–392,  
889 <https://doi.org/10.1002/lol2.10161>, 2020.

890 van Bergen, T.J.H.M., Barros, N., Mendonça, R., Aben, R.C.H., Althuisen, I.H.J., Huszar, V., Lamers, L.P.M., Lüring, M.,  
891 Roland, F., and Kosten, S.: Seasonal and diel variation in greenhouse gas emissions from an urban pond and its  
892 major drivers. *Limnology and Oceanography*, 64 (5), 2129–2139. <https://doi.org/10.1002/lno.11173>, 2019.

893 Varadharajan, C., and Hemond, H. F.: Time-series analysis of high-resolution ebullition fluxes from a stratified, freshwater  
894 lake. *Journal of Geophysical Research: Biogeosciences*, 117(G2). <https://doi.org/10.1029/2011JG001866>, 2012.

895 Velthuis, M., and Veraart, A. J.: Temperature sensitivity of freshwater denitrification and N<sub>2</sub>O emission—A meta-analysis.  
896 *Global Biogeochemical Cycles*, 36(6), <https://doi.org/10.1029/2022GB007339>, 2022.

897 Verpoorter, C., Kutser, T., Seekell, D. A., and Tranvik, L. J.: A global inventory of lakes based on high-resolution satellite  
898 imagery. *Geophysical Research Letters*, 41(18), 6396–6402. <https://doi.org/10.1002/2014GL060641>, 2014.

899 Wang, G., Xia, X., Liu, S., Zhang, S., Yan, W., McDowell, W.H.: Distinctive Patterns and Controls of Nitrous Oxide  
900 Concentrations and Fluxes from Urban Inland Waters, *Environmental Science & Technology*, 55, 8422–8431,  
901 <https://doi.org/10.1021/acs.est.1c00647>, 2021.

902 Wanninkhof, R.: Relationship between gas exchange and wind speed over the ocean. *Journal of Geophysical Research:*  
903 *Oceans*, 97, 7373–7381. <https://doi.org/10.1029/92JC00188>, 1992.

904 Webb, J.R., Clough, T.J., Quayle, W.C.: A review of indirect N<sub>2</sub>O emission factors from artificial agricultural waters,  
905 *Environmental Research Letters*, 16 043005, <https://doi.org/10.1088/1748-9326/abed00>, 2021.

906 Webb, J.R., Leavitt, P.R., Simpson, G.L., Baulch, H.M., Haig, H.A., Hodder, K.R., and Finlay, K.: Regulation of carbon  
907 dioxide and methane in small agricultural reservoirs: optimizing potential for greenhouse gas uptake.  
908 *Biogeosciences*, 16 (21), 4211–4227. <https://doi.org/10.5194/bg-16-4211-2019>, 2019.

909 Webb, J.R., Quayle, W.C., Ballester, C., Wells, N.: Semi-arid irrigation farm dams are a small source of greenhouse gas  
910 emissions. *Biogeochemistry*, 166, 123–138. <https://doi.org/10.1007/s10533-023-01100-4>, 2023.

911 Weiss, R. F., Price, B. A.: Nitrous oxide solubility in water and seawater. *Marine chemistry*, 8(4), 347–359.,  
912 [doi.org/10.1016/0304-4203\(80\)90024-9](https://doi.org/10.1016/0304-4203(80)90024-9), 1980.

913 Weiss, R. F.: Determinations of carbon dioxide and methane by dual catalyst flame ionization chromatography and nitrous  
914 oxide by electron capture chromatography. *Journal of Chromatographic Science*, 19, 611–616.  
915 <https://doi.org/10.1093/chromsci/19.12.611>, 1981.

916 West, W.E., Coloso, J.J., and Jones, S.E.: Effects of algal and terrestrial carbon on methane production rates and methanogen  
917 community structure in a temperate lake sediment. *Freshwater Biology*, 57, 949–955.  
918 <https://doi.org/10.1111/j.1365-2427.2012.02755.x>, 2012.

919 Wik, M., Crill, P. M., Varner, R. K., and Bastviken, D.: Multiyear measurements of ebullitive methane flux from three  
920 subarctic lakes. *Journal of Geophysical Research: Biogeosciences*, 118:791 1307–1321.  
921 <https://doi.org/10.1002/jgrg.20103>, 2013.

922 Xie, S., T Xia, T., H Li, H., Y Chen, Y., W Zhang, W. , 2024, Variability in N<sub>2</sub>O emission controls among different ponds  
923 within a hilly watershed, *Water Research*, 267, 122467, <https://doi.org/10.1016/j.watres.2024.122467>, 2024.

924 Xun, F., Feng, M., Ma, S., Chen, H., Zhang, W., Mao, Z., Zhou, Y., Xiao, Q, Wu, Q. L., and Xing, P.: Methane ebullition  
925 fluxes and temperature sensitivity in a shallow lake. *Science of The Total Environment*, 912, 169589.  
926 <https://doi.org/10.1016/j.scitotenv.2023.169589>, 2024.

- 927 Yan, X., Xu, X., Ji, M., Zhang, Z., Wang, M., Wu, S., Wang, G., Zhang, C., and Liu, H.: Cyanobacteria blooms: A neglected  
 928 facilitator of CH<sub>4</sub> production in eutrophic lakes. *Science of the total environment*, 651, 466-474.  
 929 <https://doi.org/10.1016/j.scitotenv.2018.09.197>, 2019.
- 930 Yang, Z., Zhao, Y., and Xia, X.: Nitrous oxide emissions from *Phragmites australis*-dominated zones in a shallow lake.  
 931 *Environmental pollution*, 166, 116-124. <https://doi.org/10.1016/j.envpol.2012.03.006>, 2012.
- 932 Yentsch, C.S., and Menzel, D.W.: A method for the determination of phytoplankton chlorophyll and phaeophytin by  
 933 fluorescence. *Deep Sea Research and Oceanographic Abstracts*, 10. Elsevier, pp. 221–231.  
 934 [https://doi.org/10.1016/0011-7471\(63\)90358-9](https://doi.org/10.1016/0011-7471(63)90358-9), 1963.
- 935 Zhao, K., Tedford, E.W., Zare, M., and Lawrence, G.A.: Impact of atmospheric pressure variations on methane ebullition  
 936 and lake turbidity during ice - cover. *Limnology and Oceanography Letters*, 6(5), 253-261.  
 937 <https://doi.org/10.1002/lol2.10201>, 2021.
- 938